A Climatological Analysis of Upper-Level Velocity Potential using Global Weather Reanalysis, 1959-2020

Tyler J. Stanfield [a] and Craig A. Ramseyer [b]

[a] *National Weather Service, Slidell, Louisiana*

[b] *Department of Geography, Virginia Polytechnic Institute and State University, Blacksburg, Virginia*

Corresponding author: Tyler J. Stanfield, tyler.stanfield@noaa.gov

Keywords: velocity potential, climate teleconnections, reanalysis, tropical variability

Abstract

Upper-level (200 hPa) velocity potential (VP200) is useful in identifying areas of rising or sinking atmospheric motions on varying temporal scales (e.g., weekly, seasonal, interannual) especially in the global tropics. These areas are associated with enhancement (rising motion) or suppression (sinking motion) of tropical convection and subsequent weather phenomena dependent on these processes (e.g., tropical cyclones). This study employed commonly used global weather reanalysis datasets to calculate and compare VP200 on interannual through multidecadal temporal scales and quantify any differences that existed between them from 1959 to 2020 over four key regions of tropical variability (Equatorial Africa, Amazon Basin, Equatorial Central Pacific, and Equatorial Indonesia). To supplement this analysis, the highly correlated variables to VP200 of outgoing longwave radiation (OLR) and daily precipitation rate were used and directly compared with independent OLR and precipitation datasets to determine the reanalysis' level of agreement with the independent data. The ECMWF ERA5 held the highest agreement to these data over all regions examined and was reasoned to have the highest confidence in accurately capturing the variability of VP200 fields for the study period. Confidence was decreased in the usefulness of the NCEP/NCAR Reanalysis 1 as it consistently performed poorly over much of the study domain. The results of this study also emphasized the usefulness in ensemble-based approaches to assess climate variability and understanding of potential biases and uncertainties that are inherent in these data sources.

Significance Statement

Global weather reanalysis datasets are vital in today's research investigating climate change and variability because they provide the most complete picture of how the atmosphere has varied over time. This study examined how well the history of upper-level velocity potential (VP200) was captured in commonly used reanalysis datasets over four key regions of tropical variability. The variable of VP200 is useful in identifying areas of rising or sinking atmospheric motions which are associated with enhancement (rising) or suppression (sinking) of tropical convection and subsequent weather phenomena dependent on these processes (e.g., tropical cyclones). The results of this study emphasized the usefulness of ensemble-based approaches in assessing climate variability and understanding potential biases and uncertainties that can be found in individual data sources.

1. Introduction

For much of the twentieth century there were no comprehensive global atmospheric reanalysis datasets capable of tracking the behavior of large-scale atmospheric motions at longer temporal scales. However, this changed with the inception of the National Centers for Environmental Prediction and National Center for Atmospheric Research (NCEP/NCAR) Reanalysis 1 (R1) dataset which inspired a new generation of study into the global circulations and their variability over time (e.g., Kalnay, 1996, Chelliah and Bell, 2004, Tanaka et al., 2004, and Kinter et al., 2004). Atmospheric reanalysis datasets provide the most complete picture of past weather and climate available today. These datasets are constructed by blending observations using short-range forecasts of past weather and satellite data using modern weather modeling data assimilation capabilities which mimic day-to-day weather forecasts. This enables the reanalysis data to fill in gaps and create a more spatially consistent product over time.

Since the variability of climate teleconnection patterns are observed on longer temporal scales (e.g., interannual, decadal), it can be challenging to fully understand their scope and impact in real-time. Applications that have made climate teleconnections in the tropics more relevant on smaller temporal scales have been through the establishment of a relationship between 200 hPa velocity potential fields (VP200), which describes the magnitude of upper-level atmospheric divergence, and the variability of tropical overturning circulations (TOCs) (Trenberth, Stepaniak, and Caron, 2000; Emanuel, Neelin, and Bretherton, 1994). Through this relationship, subsequent literature discussed the relationship between VP200 and tropical precipitation. These applications increased interest in better understanding how climate teleconnections impact the magnitude and variance in tropical precipitation over time (Zhang, Wallace, and Battisti, 1997; Higgins et al., 2000). These findings have brought about renewed research interest regarding how the evolution of the Global Walker Circulation (GWC) and subsequent teleconnections impact real-time weather in the tropics (Zaitchik, 2017; Zhang and Wang, 2021). Therefore, by analyzing how well VP200 captures the variability of the GWC and other TOCs, and their impact on tropical precipitation, these findings aim to emphasize the value in further exploring the intersection of climate teleconnections and tropical meteorology.

Since the establishment of the NCEP/NCAR R1 dataset, significant progress has been made in better understanding the evolution of Earth's atmosphere on longer temporal scales (Held, 2019). This study intends to revisit the topic of how tropical circulations are tracked through the variability of VP200 and incorporates commonly used weather reanalysis datasets (e.g., ECMWF ERA5, JRA-55, MERRA-2) to create an ensemble in climatological means and compare to the NCEP/NCAR R1 dataset's VP200. With the NCEP/NCAR R1 dataset being the primary data source for much of the early foundational literature regarding this topic, it is imperative that these findings are reproducible across other datasets, and that any observed marked differences are noted. By conducting this analysis, further research can then be more confidently conducted regarding its applications to climate teleconnections, tropical cyclone activity, and tropical convection using ensemble-based approaches or the better performing weather reanalysis datasets identified (Hersbach et al., 2020).

This research aims to provide a climatological analysis of VP200 for the 1971 to 2000, 1981 to 2010, and 1991-2020 climate periods as well as analyze the variability of the anomaly fields from 1959 through 2020. Variability of the TOCs are a primary topic of interest because it is coupled to many aspects of tropical atmospheric phenomena (e.g., El Niño-Southern Oscillation (ENSO), monsoonal circulations, and tropical cyclones) (Arkin, 1982; Back and

Bretherton, 2006). The primary circulations that drive convective activity in the tropical regions are the Hadley circulation (meridional), Global Walker Circulation (zonal), and monsoonal circulations such as the Indian monsoon (Gill, 1980; Held and Hou, 1980; Walker, 1930; Hsu and Plumb, 2000). In this study, varying temporal scales (e.g., running 1-year, 5-year, and 10-year means) were used to examine how VP200 captures climate variability in the tropics using several commonly used global weather reanalysis datasets. The interdecadal (both 5 and 10-year) temporal scale will filter the VP200 to primarily focus on the signal associated with leading TOCs, primarily the Global Walker Circulation (e.g., rising cells over the Maritime Continent, Amazonian Monsoon region, and African Continent, sinking cells over the eastern Pacific, eastern Atlantic, and Indian Ocean). Prior literature found that these circulations can be defined by their areas of upper-level divergence and convergence in the horizontal (Trenberth, Stepaniak, and Caron, 2000). This specific attribute is captured by velocity potential (χ) which is defined as a scalar field that describes the divergent, irrotational component of the horizontal velocity field (American Meteorological Society, 2022). In this case, the divergent wind measures the spreading out of the flow:

$$\vec{V}_{div} = \nabla\chi$$

Equation 1. Atmospheric divergent wind (m/s) as it relates to velocity potential (10^5 m^2/s) (Krishnamurti, 1971).

The specific component of the wind vector represents the gradient of the velocity potential which uses the horizontal wind vector at the 200 hPa level (Krishnamurti, 1971). Therefore, VP200 is proportional to divergence where areas of positive (negative) VP200 are associated with convergence (divergence) aloft and subsequent subsidence (rising motion).

With the usefulness of VP200 in depicting the intensity and size of atmospheric divergence and convergence aloft, further studies were conducted in understanding how these extrema in VP200 were associated with variability in tropical precipitation via intraseasonal oscillations (e.g., Madden-Julian Oscillation) and their inherent association to the TOCs (Lau, D. E. Waliser, and D. Waliser, 2005; Jiang et al., 2020).

Using these dynamical atmospheric properties, it has been established in prior literature that subsidence (rising motion) is associated with suppression (enhancement) of convection (Holton, 2004). Therefore, the use of VP200 was found to be a valid proxy for tracking the suppression and enhancement of tropical convection at varying temporal scales which has provided numerous applications for VP200.

2. Applications of VP200

2.1. Subseasonal to Interannual Temporal Scales

The versatility of VP200 has been shown to be useful in the tracking and prediction of tropical climate oscillations at shorter temporal scales in addition to the longer temporal scales. Such oscillations include the Madden-Julian Oscillation (MJO) which is characterized as an oscillation in trade winds and surface fluxes which enhance, or suppress, tropical convection at an average periodicity on the order of 30-60 days (Madden and Julian, 1971; 1972). Tracking the MJO is an important aspect of understanding and forecasting high-frequency variability in tropical convection and subsequent tropical cyclone activity (Roundy and Schreck III, 2009; Roundy, Schreck III, and Janiga, 2009; Ventrice et al., 2011). In addition to its short-term applications, prior studies have found MJO behavior has a strong connection to interannual variability associated with ENSO and the low-frequency variability observed with the TOCs (McPhaden et al., 2006; Hendon, Wheeler, and Zhang, 2007; Roundy et al., 2010; Roundy, 2015).

Prior methods had been employed by Wheeler and Hendon (2004) to create a tracking algorithm using Empirical Orthogonal Functions (EOF) for outgoing longwave radiation (OLR) and zonal winds (at 850 hPa and 200 hPa) to monitor the behavior of the MJO which is commonly known as the Real-time Multivariate MJO (RMM) diagram. With this, VP200 was found to be a valid replacement for OLR in the RMM algorithm and was more effective at retaining consistent MJO tracking across the tropical Pacific (Ventrice et al., 2013).

In addition to these studies, prior literature has also examined the relationships of precipitation, OLR, and VP200 between reanalysis datasets using smaller temporal domains (e.g., 1980-93) with notable disagreements that raise further questions regarding their accuracy and increase the motivation for this study (Newman, Sardeshmukh, and Bergman, 2000).

2.2. Decadal and Multidecadal Temporal Scales

The VP200 literature also helped identify the existence of multidecadal regimes in which the branches of the GWC vary (Chelliah and Bell, 2004; Tanaka et al., 2004). While the branch that encompasses the Pacific Walker circulation remains the most dominant feature in the overall background state, the weaker rising cells over South America and Africa have more notable variations over time in the reanalysis (Chelliah and Bell, 2006). This variability has had significant consequences in multidecadal climate over these regions resulting in significant periods of drought and/or flooding. These variations are largely driven by fluctuations in sea surface temperatures and land-atmosphere interactions and thus tracking these variations in near real-time is a possibility as understanding of the anthropogenic and natural mechanisms driving the TOCs increases. For instance, cooling of the eastern tropical Pacific and warming of the tropical Atlantic during the late 1990s and early 2000s resulted in strengthening of the local

Walker circulation and associated rising motion over South America. This resulted in a notable increase of severe flooding events across the Amazonian basin (Barichivich et al., 2018). Similar trends in other basins have also been attributed to modulation of individual cells within the Global Walker circulation which have implications on future climate teleconnections (Dhame et al., 2020).

The strength and behavior of the TOCs are primarily driven by the uneven distribution of diabatic heating/cooling across the tropics which are subject to change in a warming climate (Vecchi and Soden, 2007; Seidel et al., 2008). Therefore, part of understanding the circulation's variability over time also requires understanding how it will be modulated by anthropogenic climate change. Numerous studies have been conducted in the last decade examining how these changes will impact tropical circulations (Gastineau, Li, and Le Treut, 2009; Ma, Xie, and Kosaka, 2012; He and Soden, 2015). These studies conclude that the tropical circulations will weaken because of anthropogenic climate change due to the weakening global temperature gradients that drive them. With the weakening of these circulations, it is important to understand how it will impact the hydrological cycle and local climates which has been the primary focus of subsequent research (Ma et al., 2018). Further, while these results are plausible, trends in reanalysis data (e.g., ECMWF ERA-Interim, NCEP/DOE Reanalysis II, JRA-55, MERRA-2 and CFSR) do not necessarily corroborate all these climate trends compared to climate model projections (Chemke and Polvani, 2019). Findings such as these highlight the necessity for continued improvement in global atmospheric reanalysis datasets to continue to improve the ability of these reanalysis to track large-scale circulations.

3. Data and Methods

Prior literature concerning the use of VP200 in climate teleconnections and tropical meteorology have brought forth impactful outcomes in more efficient tracking of the TOCs in the global tropics. With this prior literature, new interest has been stimulated in the consistency of VP200's depiction and use across global weather reanalysis datasets. Therefore, it is imperative that new literature be established that analyzes VP200 in the global tropics across multiple reanalysis datasets to strengthen confidence in the prior conclusions established using these data and their use in future applications.

3.1. Data Sources

The three commonly used global weather reanalysis datasets that extend prior to the satellite era are the NCEP/NCAR R1, ECMWF ERA5, and JRA-55 (full-period reanalysis datasets henceforth) with a common period beginning in 1959, when upper air observations became more consistent (Table 1). These datasets are important in understanding modeled variability of VP200 given fewer observations existed to capture the variability of large-scale phenomena like the TOCs. Therefore, it was anticipated that greater discrepancies and uncertainty would exist with these data when evaluating the VP200 fields, especially over data sparse regions (e.g, tropics, oceans).

The satellite era reanalysis datasets (NCEP/NCAR R2, NASA MERRA2, and CFSR/CFSv2) were used over their full periods within the study's 1959-present temporal domain to strengthen consensus of the VP200 fields and identify what discrepancies existed with these datasets. Since NCEP/NCAR R1 (shortened to NCEP R1 henceforth) was the primary dataset used in much of the early foundational literature using velocity potential to monitor the TOCs, it was considered the control dataset to which other datasets were to be compared (Table 1). Datasets such as ERA5 and JRA-55 provide a higher spatiotemporal resolution, 4D-Var data assimilation, improved model physics, and more observations (Hersbach et al., 2019; 2020). These developments resulted in notable improvements from the NCEP R1 particularly with precipitation in data sparse regions such as equatorial Africa and South America in which further analysis with data separate from the reanalysis datasets would be necessary (Kalnay et al., 1996; Kistler et al., 2001; Kobayashi et al., 2015).

The highly correlated variables to VP200 (e.g. OLR and precipitation) were evaluated in these global weather reanalysis datasets using independent datasets. The independent precipitation data were comprised of two merged satellite-rain gauge products (i.e., CMAP and GPCP version 2.3) and a land station-based product from the Global Precipitation Climatology Centre (GPCC) as they were used in the prior literature (Chelliah and Bell, 2004; Kinter et al., 2004; Kobayashi et al., 2015). CMAP and GPCP version 2.3 have a temporal domain from 1979-2020 which was adequate for verifying much of the temporal domain. However, this left 22 years of reanalysis data with limited credible alternatives for verification in the pre-1979 portion of the study period early period (Xie and Arkin, 1997; Adler et al., 2018). To remedy this issue, the land-based rain gauge data from the GPCC precipitation dataset was used over most of the study's temporal domain in addition to the merged satellite-rain gauge products (Becker et al., 2013). It was acknowledged that using land-only observations to evaluate the performance of reanalysis-based variables was a limitation in this study. Nevertheless, few precipitation datasets were available during the pre-satellite era (1979-present), and GPCC was the most temporally complete gridded gauge-analysis product for climate analysis to date.

Mitigation of some of these limitations were addressed by using the NOAA Interpolated OLR and HIRS OLR monthly dataset that spanned from January 1979 to present to provide a tertiary source of verification to reanalysis datasets. The NOAA OLR dataset uses the Advanced Very High-Resolution Radiometer (AVHRR) instrument aboard the NOAA polar orbiting spacecraft to collect swaths of OLR data which are spatially and temporally interpolated onto grids to facilitate use (Liebmann and Smith, 1996). The HIRS OLR dataset is a newer alternative to the NOAA Interpolated with inclusion of more OLR data sources from instruments onboard NOAA TIROS-N series and Eumetsat MetOp-A/B polar-orbiting satellites to geostationary satellite estimates (Lee, Gruber, Ellingson and Laszlo, 2007; Lee, 2018; Schreck, Lee, and Knapp, 2018).

Reanalysis Ensemble	Ensemble Members
Full-period Reanalysis datasets (1959-2020)	NCEP R1, ERA5, JRA55
Satellite Era Reanalysis datasets (1980-2020)	NCEP R2, CFSR/v2, MERRA-2
NCEP Reanalysis datasets	NCEP R1, NCEP R2, CFSR/v2
Non-NCEP Reanalysis datasets	MERRA-2, JRA-55, ERA5

Table 1. Grouping of reanalysis datasets for data analysis and discussion of results based on common attributes.

3.2. Data Analysis

A climatology of global VP200 from 20ºN to 20ºS was created for all months and seasons using the 1981-2010 reference period for each reanalysis dataset, respectively. The use of temporal filtering was leveraged to reduce transition season variability. It was determined prior that DJF and JJA are the most seasonally consistent periods in the VP200 climatology, and are preferred over annual means, because they remove the strong seasonality of tropical convection and its atmospheric response that are associated with the transition seasons (Chelliah and Bell, 2004). However, to evaluate the full temporal scope of these global weather reanalysis' ability to capture climate variability, all timesteps were used in this study.

The 1981-2010 climatological means were used to calculate monthly and seasonal anomalies for VP200, outgoing longwave radiation (OLR), and daily precipitation rate (PR). Monthly climatological means and anomalies of VP200 were then used to spatially compare to the respective reanalysis' own variables (OLR and PR) and compute the correlation coefficients (r) between the reanalysis and independent precipitation and OLR datasets (e.g., CMAP, GPCP, GPCC, NOAA Interpolated OLR, and HIRS OLR). These analyses were conducted over four key tropical regions: Equatorial Indonesia [0°-10°N, 95°E-115°E], Equatorial Central Pacific [0°-10°N, 170°W-150°W], Amazonian Monsoon Region [10°S-0°, 55°W-45°W], and West African Monsoon Region [0°-15°N, 0°-30°E] (Figure 1).

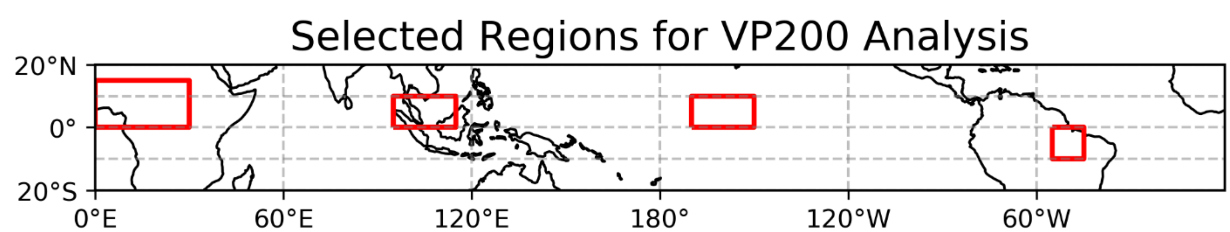

Figure 1. Study spatial domain bounded between 20°N to 20°S and red boxes denoting the domains of the four study regions analyzed further.

These regions were selected due to their noted interdecadal variance in mean precipitation which can be used to evaluate how well interdecadal variance of VP200 relates to these changes (Kinter et al., 2004). Further, these regions spatially coincide with the rising and sinking branches of the Global Walker Circulation which would capture variability of the TOCs through the study period. To supplement the reasoning for analyzing these regions further, 30^{o} longitudinal moving averages (at intervals of 10^{o} bounded between 20^{o}S to 20^{o}N) were calculated for VP200 of each global weather reanalysis dataset to provide a more spatially complete analysis of the locations of the strongest agreement via correlation coefficient between reanalysis datasets.

VP200, PR, and OLR anomalies were temporally filtered at 1-year, 5-year, and 10-year moving averages for each study region to evaluate variability for all data sources using time series plots. These filtered data were purposed with identifying periods of clear disagreement between the data sources to better understand periods of higher uncertainties and illustrate the variance in reanalysis' depiction of the TOCs over time (Tanaka et al., 2004). Pearson correlation coefficients were computed for all temporally filtered data in addition to the unfiltered data to analyze linear relationships that may exist between the regions on varying temporal scales. This allowed for thorough analysis of the dataset's depiction of the TOCs' behavior by quantifying the level of consilience, identifying any nuanced differences between the datasets not initially evident, and forming stronger conclusions.

4. Results and Discussion

The synopsis of the results is detailed in this section with more detailed discussion of findings given in the following subsections. VP200 in the global tropics is captured most effectively in the western equatorial Pacific where ENSO variability is dominant and spatiotemporal observations have covered the study period sufficiently (Figure 2). Significant discrepancies in the reanalysis datasets exist in data sparse regions such as tropical South America and Africa especially prior to the satellite era (i.e., prior to 1979). These areas are where confidence in the reanalysis datasets' capturing of VP200 are lowest given the lack of strong consensus between them. This highlights the need to examine multiple reanalysis datasets in these regions to provide a range of possible solutions instead of focusing on any one reanalysis dataset.

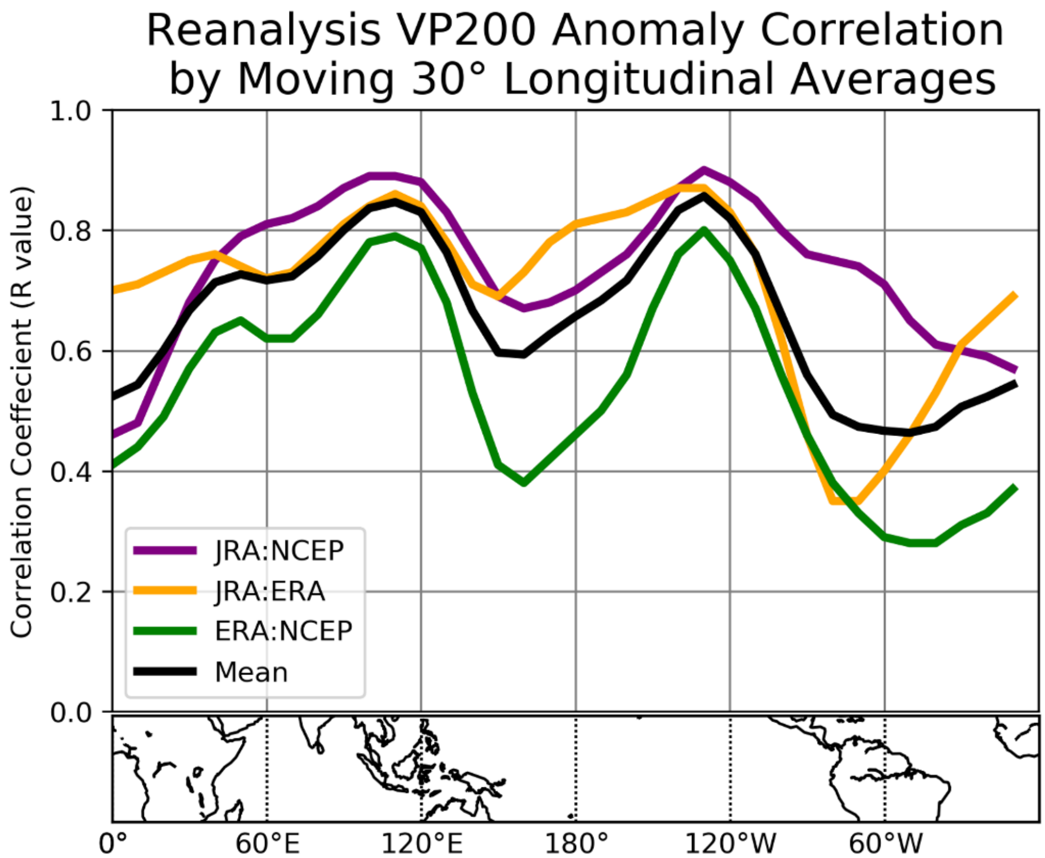

Figure 2. R-values of 30º longitudinal averaged regions bounded between 20ºN to 20ºS to describe the level of agreement of global weather reanalysis upper-tropospheric velocity potential fields (1958-2020).

The results of this study indicate ERA5 had significant improvement in performance with the independent precipitation and OLR datasets compared to the NCEP R1. This makes its use in future research of VP200 more viable with acknowledgement to the noted biases it could still have based on the precipitation and OLR analysis. Alternatively, the NCEP R1's depicted variability in VP200 especially over the South American and African continents was not physically supported by any other data source used in this study. NCEP R1 also observed a much higher climatological mean value (i.e., stronger upper-level convergence and subsequent sinking motion) over tropical Africa compared to the JRA-55 and ERA5 which was likely the cause of the more anomalous negative (i.e., stronger upper-level divergence and subsequent upward motion) VP200 anomalies in recent decades. These discrepancies did not improve much with NCEP R2 when compared to the full suite of reanalysis datasets available in the satellite era. Finally, climatological means of VP200 over the last three climate periods (i.e., 1971-2000, 1981-2010, and 1991-2020) appeared to become more similar between reanalysis datasets which precludes any conclusive anthropogenic climate signals that could be identified in this analysis.

4.1. 30 Degree Moving Longitudinal Averages

In addition to the four study regions selected for further analysis of VP200, supplemental analysis was performed on 30º moving longitudinal averages bounded between 20ºS to 20ºN to provide spatial continuity in evaluating full-period reanalysis agreement in VP200 across the global tropics. Data analysis was also performed using 5-year and 10-year filters to remain temporally consistent with the analysis by region. The correlations (r) between these reanalysis averages were used to determine the level of agreement and found highest correlations in the western (90-150ºE) and eastern (220-270ºE) tropical Pacific where mean correlation coefficients exceeded 0.80 (Figure 2).

This was physically consistent given the high explained variance associated with ENSO in both areas due to the proximity of the rising and sinking branches of the Pacific portion of the Global Walker Circulation (Oliver, 2005). The lowest correlations (Mean $r < 0.60$) were located over the central tropical Pacific (150-190ºE) and tropical South America through tropical Africa (270-50ºE). Correlations between JRA-55 and ERA5 were comparatively highest over tropical

Africa and central tropical Pacific while correlations between NCEP R1 and ERA5 were comparatively lowest across nearly all areas. Correlations between JRA-55 and NCEP R1 were highest over the western and eastern tropical Pacific as well as tropical South America where ERA5 clearly differed the most from the other two reanalysis (See Appendix A: Table A1). These results provided increased confidence in the reasoning behind the selection of the four study regions analyzed further. More specifically, the clear disagreements noted in this analysis over open ocean (Central Equatorial Pacific) and in data sparse regions (Equatorial Africa and Amazon Basin) enhanced the motive to further investigate how large these differences were and why they may be occurring over these areas.

4.2. Climatological Trends in VP200 Reanalysis Datasets

The annual and monthly climatological means for each reanalysis dataset were calculated over the four study regions selected for further analysis of long-term changes. Understanding reanalysis estimation of climatological averages in VP200 was crucial in identifying disparities in the reanalysis data as well as any statistically significant trends over time. While the primary climatology in this study was 1981-2010, the annual and monthly climatological means of 1971-2000 and 1991-2020 were also calculated for each region to provide better context regarding reanalysis climatological means (Table A2). The largest disparities in monthly climatological means were during each region’s respective warm season (boreal summer – JJA, austral summer – DJF) with the strongest agreement occurring in the cold season (Figure 3). Further, variability in the monthly climatological means within each region sufficiently captured the expected variance in values caused by movement of the Hadley cell between hemispheres. The most consistent conclusion from all four regions was that climatological means began with more disagreement in the 1971-2000 climatology and were converging to form a stronger consensus of means by 1991-2020 (Figure 4). These adjustments in climatological means also emphasized the need for caution in associating these trends with anthropogenic forces without further examination using other data sources.

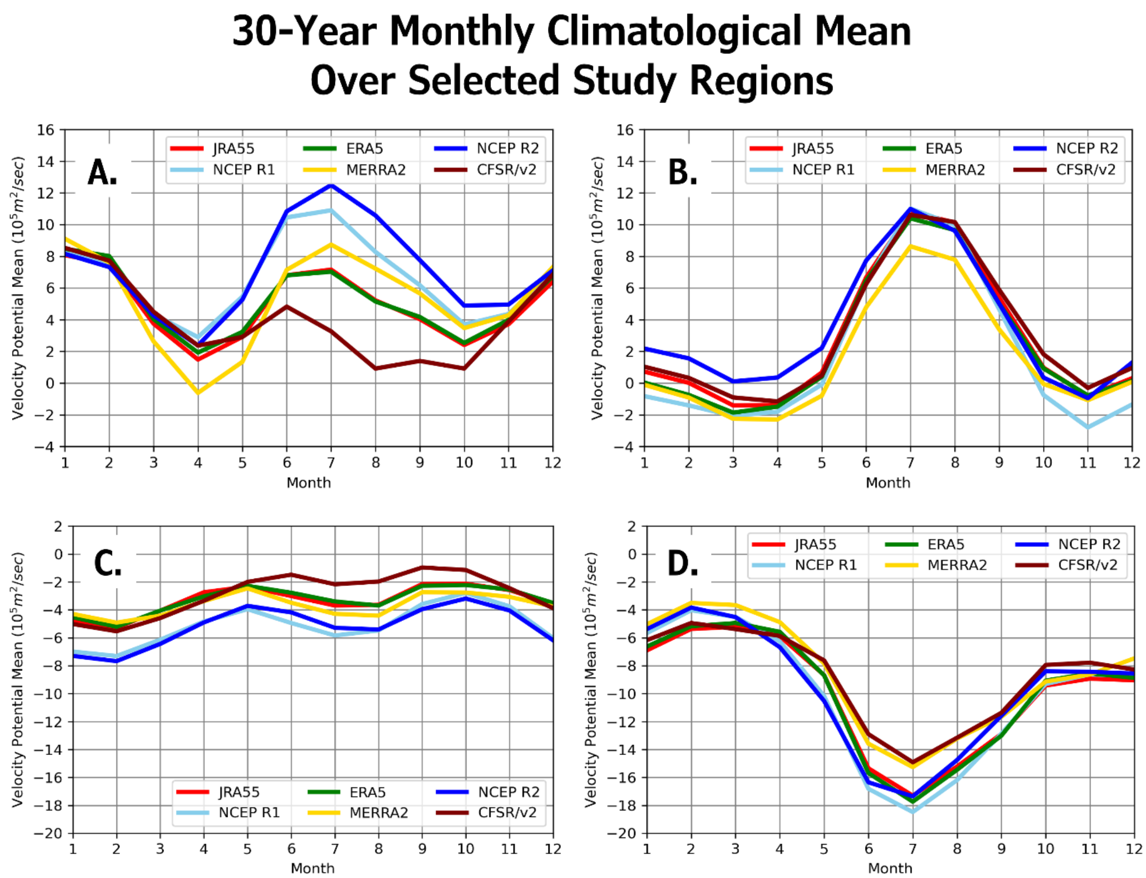

Figure 3. 1981-2010 monthly climatological means of VP200 over (A.) Equatorial Africa, (B.) Amazon Basin, (C.) Equatorial Central Pacific, and (D.) Equatorial Indonesia for each global weather reanalysis dataset.

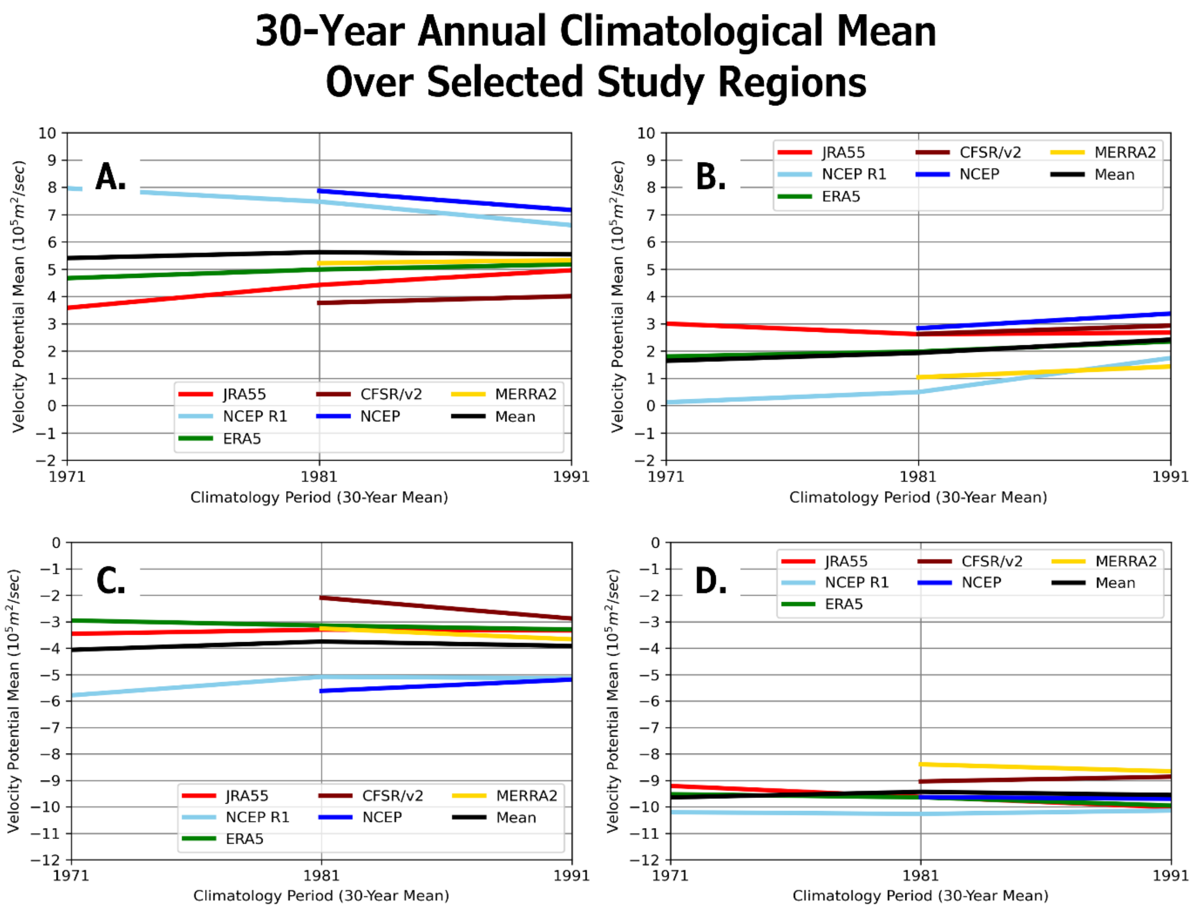

Figure 4. Annual climatological means of VP200 over (A.) Equatorial Africa, (B.) Amazon Basin, (C.) Equatorial Central Pacific, and (D.) Equatorial Indonesia for each global weather reanalysis for the last three 30-year climate periods (1971-2000, 1981-2010, 1991-2020).

Examining the spatial consistency of the climatological means for DJF and JJA supplemented understanding of how the reanalysis data varied and influenced the quantified differences (Figure 5). The areas with largest spatial variance between reanalysis during DJF (austral summer) were in association with the northward extent of Pacific Walker circulation (and Hadley cell) and the Amazon monsoon circulation’s strength.

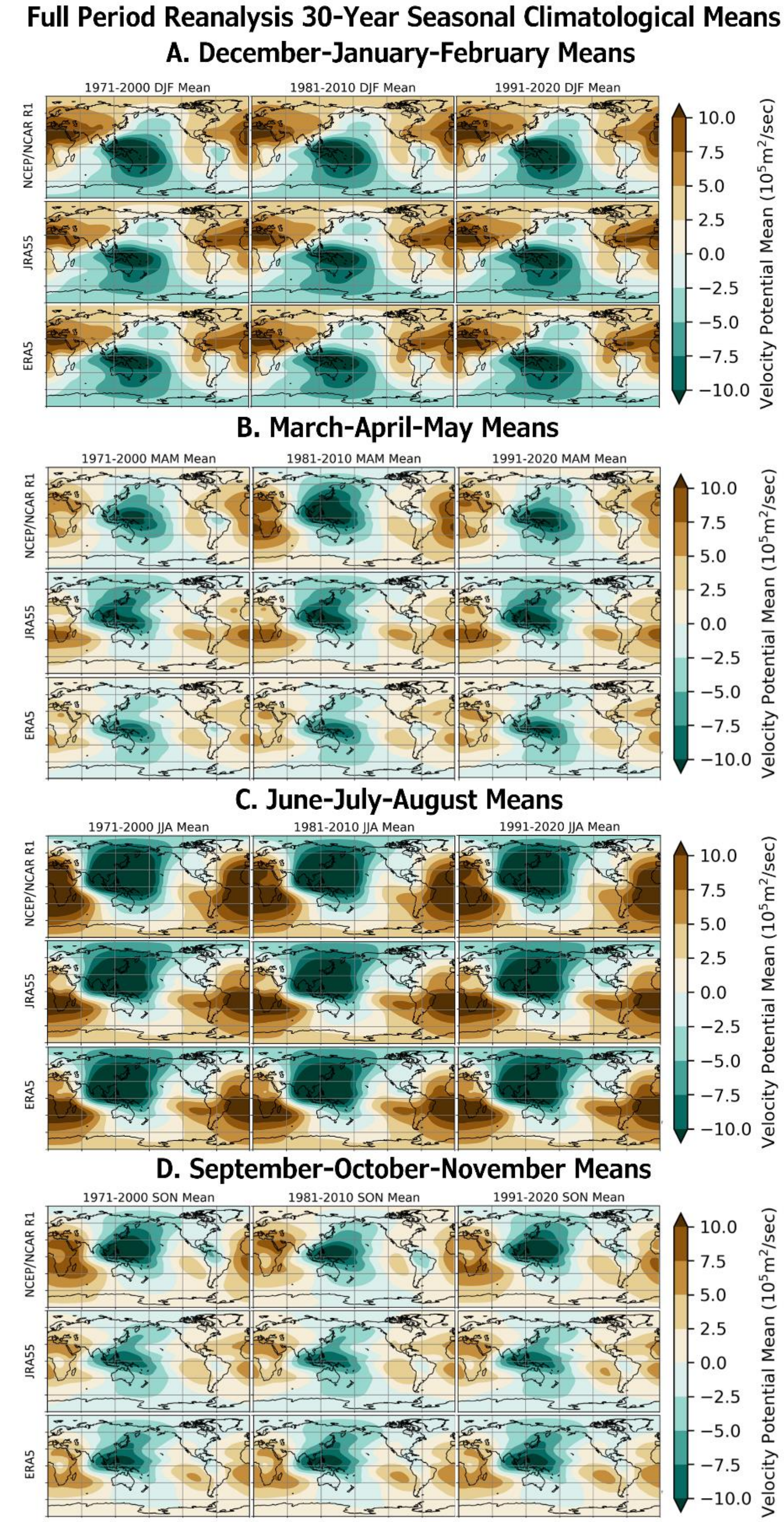

Figure 5. Panel of VP200 seasonal means for the last three 30-year climate periods depicted in each of the full period (1959-2020) reanalysis datasets. (A) December-January-February means, (B) March-April-May means, (C) June-July-August means, and (D) September-October-November means.

The NCEP R1 exhibited some of the largest deviances from the ensemble mean throughout this analysis. One potential cause is that NCEP R1 depicted a more expansive Pacific Walker circulation across the central Pacific than the modern reanalysis datasets (ERA5, JRA-55, and MERRA2). It also had a more negative VP200 mean over the Amazon basin region indicative of a stronger rising cell especially in the earlier climate periods. Substantial spatial differences between NCEP R1 and the modern reanalysis datasets were observed over North Africa during JJA where the NCEP R1's means were much higher. Other nuanced differences were also observed with the eastward extent of the rising cell of the Pacific Walker circulation with the NCEP R1 extending slightly more east in the central Pacific than the modern reanalysis datasets. Given this issue extended to DJF, it could provide an explanation as to why the NCEP R1 means were consistently more negative for all climate periods.

4.2A. Equatorial Africa

Notable disparities were observed in the annual climatological VP200 means of full-period reanalysis datasets for each 30-year average where NCEP R1 ranged from 8.0 (*10^5 m2/s) in 1971-2000 to 6.6 in 1991-2020, JRA-55 3.6 to 5.0, and ERA5 4.6 to 5.2 by 1991-2020 (Table A2). These differing trends in values were assumed to be a symptom of early period biases in which means were converging toward a consensus climatological value (Figure 4A). The ERA5 and JRA-55 trend could be anthropogenically influenced, or it may be a result of a bias in the respective models. Further, the statistical significance of the differences was not strong enough to consider further investigation nor was this aspect the primary motive for this study.

There were differences observed across several months, especially in the 1971-2000 means, when analyzing the monthly VP200 climatological means. However, it was observed that stronger consensus had developed between JRA-55 and ERA5 for all months by 1991-2020. The most significant disparity was in the boreal summer months between the modern reanalysis datasets and the NCEP R1 in which 1981-2010 monthly values differed by over 5.0 (*10^5 m2/s) during JJA. These values appeared to be decreasing with each successive climatological mean which gave stronger confidence in the JRA-55 and ERA5 consensus being closer to a representative climatological average for both annual and monthly means (Figure 3A).

This region's monthly means observed a bimodal peak in VP200 during DJF and JJA with values climatologically most negative during transition seasons which is likely strongly influenced by movement of the rising branch of the Hadley cell between each hemisphere. This is physically consistent given that the West African Monsoon is active during the warm season and the Intertropical Convergence Zone (ITCZ) is typically located north of this region (Raj et al. 2019; Geen et al. 2020).

4.2B. Amazon Basin

The annual climatological means of full-period reanalysis datasets for the Amazon Basin region were initially in less agreement in the 1971-2000 means with JRA-55 at 3.0 (*10^5 m2/s), ERA5 at 1.8, and NCEP R1 near 0 (Table A2). However, by 1991-2020 these means had converged with JRA-55 near 2.7, ERA5 at 2.3, and NCEP R1 at 1.7 (Figure 4B). Given the magnitude of changes in the climatological means across the three periods, it suggested that NCEP R1 was furthest from the consensus climatological mean initially. This region was the only to observe a majority of reanalysis datasets trending positive in VP200 annual means which could be investigated further as an anthropogenically driven climate trend given the adverse changes in land types being observed in the Amazon (Alves de Oliveira et al. 2021).

The seasonal variability of VP200 in monthly climatological means for each reanalysis were generally in agreement. The largest differences occurred during austral summer months with NCEP R1 means consistently more negative than the newer reanalysis datasets (Figure 3B). MERRA-2 also had a lower austral winter peak in monthly means compared to other reanalysis datasets. The variability of the monthly means over the region effectively captured the expected behavior of southern hemisphere Hadley cell propagation with values most negative during DJF and most positive during JJA. These monthly means were also indicative of the annual means behavior in which a stronger consensus was made apparent with the 1991-2020 monthly means. ERA5 appeared to be the most consistent reanalysis between climatological means as it held the highest agreement to the ensemble reanalysis mean of climatological means.

4.2C. Equatorial Central Pacific

There were some converging trends observed from the 1971-2000 to 1991-2020 annual VP200 climatological means in this region, but also a notable disparity involving NCEP R1 and NCEP R2. Modern reanalysis datasets were generally between -3.0 and -3.7 (*10^5 m2/s) while NCEP R1 and NCEP R2 annual means were between -5.1 to -5.8 (Table A2).

The monthly climatological means observed a bimodal peak inverse to Equatorial Africa where mean values were highest during the transition seasons and lowest during DJF and JJA. This variability, while influenced by the Hadley cell, was also evidently influenced by the GWC in which transition season forces are weakest along the equatorial Pacific (Figure 3C).

The NCEP R1 and NCEP R2 were as much as 2.7 (*10^5 m2/s) lower in mean value compared to the modern reanalysis. The disparity present with the NCEP reanalysis datasets warranted further interrogation to determine potential causes and diagnose any bias that may exist in this region. It was postulated that the consistent negative bias in the NCEP reanalysis datasets for this region was due to the significantly anomalous negative values observed in the early period (e.g., 1958-1979). If NCEP R1 and R2 were removed from the reanalysis datasets means, it was noted there was a subtle negative slope to ERA5, MERRA-2, and CFSR/v2 that could point to either a wetting bias or anthropogenic trend (Figure 4C).

4.2D. Equatorial Indonesia

The annual climatological means over Equatorial Indonesia demonstrated the highest agreement over the period with the JRA55 and ERA5 gradually decreasing and settling close to NCEP R1 at around -10.0 ($*10^5$ m^2 s^{-1}) (Table A2). Again, given that early discrepancies existed between the datasets, it was much harder to diagnose any substantive anthropogenic climate trends in these data and rather represent a convergence of the reanalysis data toward a consensus climatological mean value (Figure 4D).

Monthly climatological means over the region depicted a strong seasonality of the VP200 in association with movement of the Hadley cell and respective rising branch of the GWC (Figure 3D). Means were spread largest during boreal summer illustrating the increased uncertainty in modeled behavior when more widespread tropical convection was present. This range decreased over time as indicated by the annual means calculated using the 1991-2020 monthly means that formed a stronger consensus for all months (Table A2). This led to the Equatorial Indonesia region as the region with the highest confidence (e.g., consensus) in the VP200 for the entire period analyzed.

4.3. Velocity Potential Variability Analysis by Region

While Section 4.2. analyzed each region's climatological VP200 means, this section will present each region's VP200 anomalies. These anomalies were analyzed with 1-year, 5-year, and 10-year temporal filters to provide a suite of visualizations depicting interannual, decadal, and multidecadal agreement between reanalysis datasets (Tables A3 and A4). NCEP reanalysis datasets (i.e., CFSR/v2, NCEP R1, and NCEP R2) had the largest disagreements to the non-NCEP reanalysis datasets (i.e., ERA5, JRA-55, and MERRA-2) over the Equatorial Africa and Amazon Basin regions throughout the period in all filtered temporal scales. Lower magnitude differences were depicted in the Equatorial Indonesia region with additional disagreement in anomaly values apparent in the early period between NCEP R1 and the newer reanalysis in the Equatorial Central Pacific region.

4.3A. Equatorial Africa

Low agreement existed in all temporally filtered monthly anomalies in the Equatorial Africa region analyzed for the pre-satellite period (Figures 6A and 6B). While the newer reanalysis increased in agreement beginning in the late 1980s, the NCEP R1 and R2 anomalies seldom agreed with them. More specifically, JRA55 and NCEP R1 anomalies appeared to even have more inverse behavior in the 5-year and 10-year filtered anomalies with more positive NCEP R1 anomalies from the late 1970s until the late 1990s while JRA-55 possessed more negative anomalies during this period.

The NCEP R1 flipped to more negative values, like values in the 1950s and 1960s, during the last two decades of the study period which had been leveraged as a potential multidecadal signal in the past (e.g., Bell and Chelliah, 2006). This was not supported by newer reanalysis data with ERA5, MERRA-2, and CFSR (prior to CFSv2 extension) bounded more closely to zero than the NCEP R1, NCEP R2, and JRA-55. Some decadal and interannual behaviors are observed throughout the period, however, the disagreement in magnitude and sign amongst the datasets increased the difficulty in diagnosing such variability especially prior to 1990 (Figures 7A and 7B).

4.3B. Amazon Basin

Some of the most conclusive evidence in identifying differences between the reanalysis datasets was found in the Amazon Basin region. Across all temporally filtered monthly anomalies, the NCEP R1 values were notably different in comparison to the JRA-55 and ERA5 for the entire period (Figure 6C). The 5-year and 10-year filtered anomalies make this discrepancy more evident as the NCEP R1 possessed anomalously higher values for much of the early period before 1980 (Figure 6D).

These values then became anomalously more negative than the newer reanalysis datasets from 1980 to 2000 before becoming anomalously more positive once more during the last two decades of the study period. NCEP R1's behavior was far more variable over the temporal domain compared to the newer reanalysis datasets and provided compelling evidence toward the uncertainty of the NCEP R1 over this region. These large discrepancies appear to be reduced in the satellite era with the NCEP R2 and are in better agreement with the ERA5, MERRA-2 and JRA-55 which held the highest agreement with one another in this region (Figures 7C and 7D).

4.3C. Equatorial Central Pacific

The Equatorial Central Pacific region exhibited a similar signal as the previous sections as NCEP R1, NCEP R2, and CFSR/v2 data exhibited larger differences than the newer reanalysis datasets, especially with NCEP R1 in the early period prior to the satellite era. VP200 monthly anomalies in the NCEP R1 were consistently anomalously more negative during the pre-satellite era before converging into a much tighter consensus with the other reanalysis datasets (Figures 6E and 6F).

The behaviors captured especially in the 1-year filtered anomalies were directly associated with ENSO variability with negative anomalies associated with warmer ENSO while positive anomalies occurred during cooler ENSO events (Figure 7E). The 5-year and 10-year filtered anomalies after 1979 were more tightly agreed upon and thus captured a reasonable consensus in decadal and multidecadal variability in ENSO behavior during this period (Figure 7F).

4.3D. Equatorial Indonesia

The region with strongest consensus amongst all reanalysis datasets employed in this study was Equatorial Indonesia. General agreement was observed through much of the study period with only subtle differences in magnitude.

ENSO variability was also captured in this region in the 1-year filtered anomalies with a sign opposite to the Equatorial Central Pacific region given its placement on the other side of the Pacific Walker circulation (Figures 6G and 7G). However, more noticeable disagreement was identified between NCEP and non-NCEP reanalysis datasets in the 5-year and 10-year anomalies

(Figures 6H and 7H). Most notably, the NCEP reanalysis datasets had more negative values in the late 1980s to mid-1990s which then became more positive from the mid-2000s until 2020. While ERA5 and JRA-55 held the highest agreement with each other, it was observed that both began above the ensemble mean of anomalies at the beginning of the period before becoming more negative in the 2005-2015 period indicating the potential existence of a wetting bias in this region. These datasets also agreed best with the MERRA-2 which appeared to remain closer to the ensemble mean of anomalies through the period. Regardless, this supports the reanalysis ensemble mean approach countering individual dataset biases with the objective of providing a representative depiction of VP200 variability over the region.

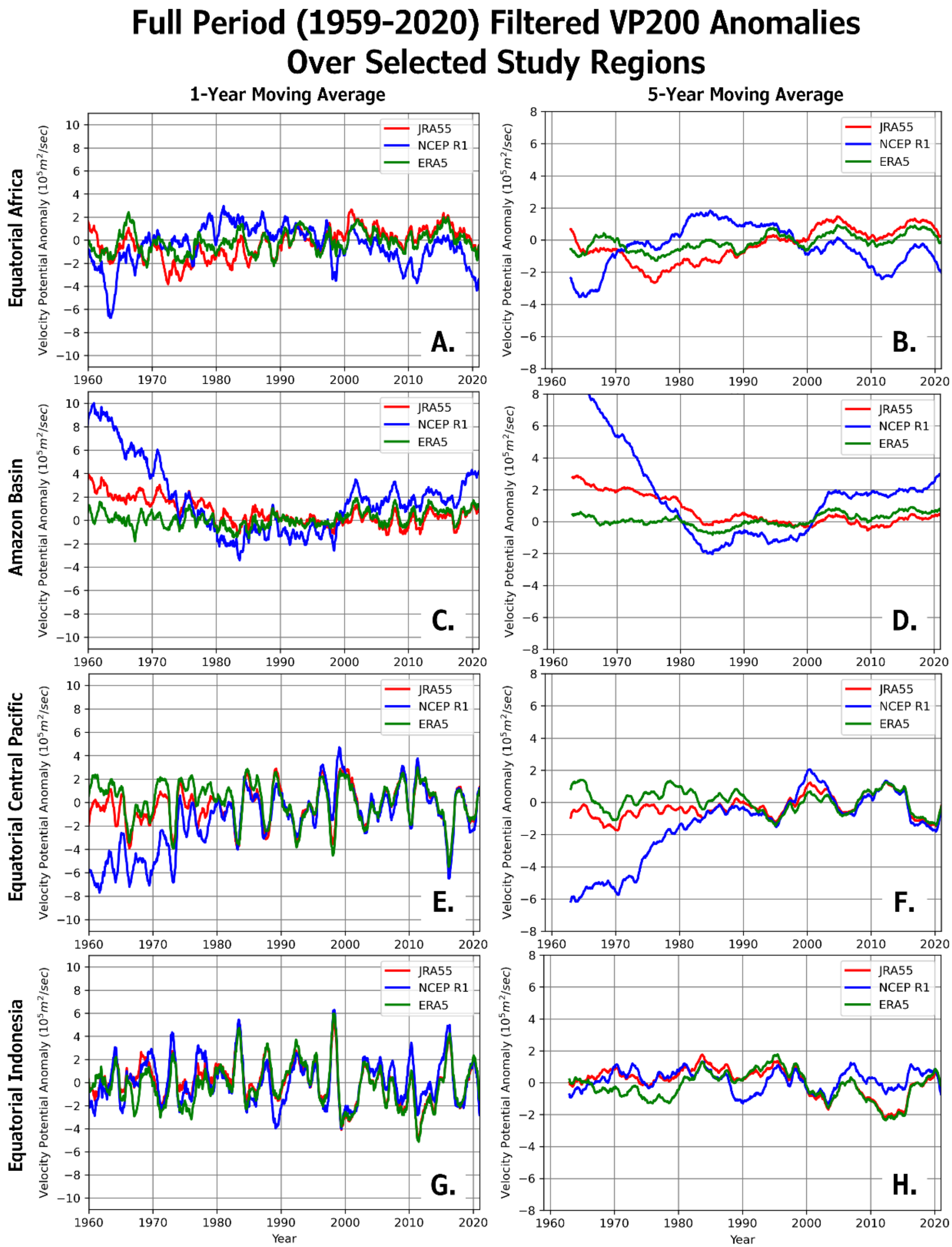

Figure 6. 1-year (left) and 5-year (right) filtered (moving average) of VP200 anomalies of each full period global weather reanalysis dataset over (A. and B.) Equatorial Africa, (C. and D.) Amazon Basin, (E. and F.) Equatorial Central Pacific, and (G. and H.) Equatorial Indonesia.

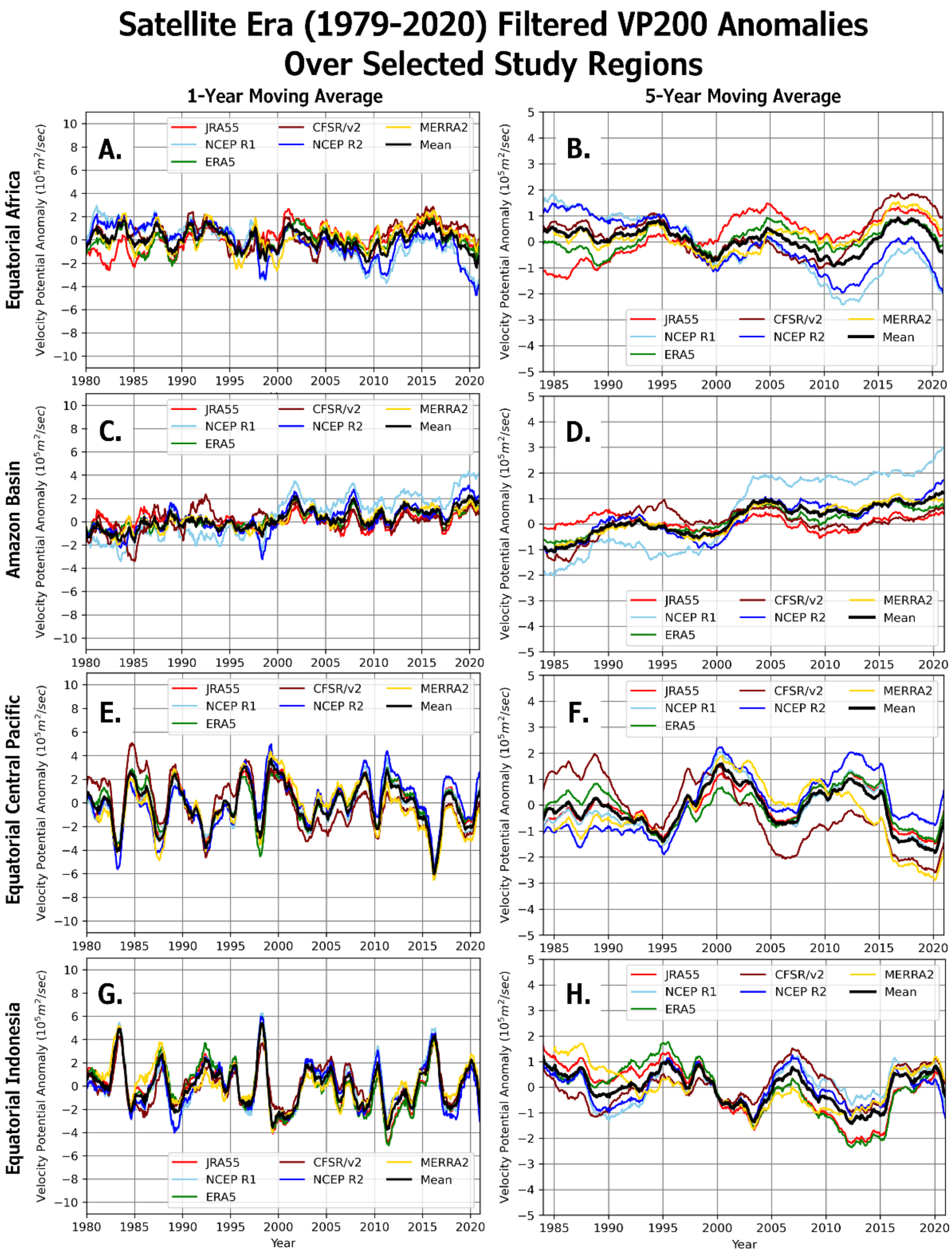

Figure 7. 1-year (left) and 5-year (right) filtered (moving average) of VP200 anomalies of each global weather reanalysis dataset for only satellite era over (A. and B.) Equatorial Africa, (C. and D.) Amazon Basin, (E. and F.) Equatorial Central Pacific, and (G. and H.) Equatorial Indonesia.

4.4. Reanalysis Performance with Independent Datasets

The monthly VP200 anomalies calculated for varying, filtered temporal scales yielded notable disagreements that warranted further investigation using independent OLR and precipitation datasets (i.e., not leveraged in the data assimilation schemes for the reanalysis data). The behaviors exhibited by the VP200 anomalies from the reanalysis datasets were compared to the respective reanalysis OLR and precipitation anomalies (e.g., negative (positive) OLR and positive (negative) PR anomalies were associated with negative (positive) VP200 anomalies). These reanalysis OLR and PR anomalies were then directly compared to independent datasets to form a stronger conclusion and diagnose potential biases that exist with these reanalysis datasets in each region.

4.4.1. Precipitation

ERA5 consistently performed the best (i.e., highest R-value in respective study regions) among the reanalysis datasets especially in the Amazon Basin region while NCEP R1 performed the worst. There was generally strong agreement between the independent precipitation datasets across all regions with Equatorial Africa having the weakest agreement. Further, it was acknowledged a potential caveat in this analysis was the CMAP's use of NCEP/NCAR reanalysis to interpolate precipitation values which could create bias in favor of NCEP reanalysis datasets in this performance analysis, especially in the pre-satellite era. This performance analysis was also temporally limited due to the differences in temporal domains of these independent datasets. Therefore, the analysis of independent precipitation data was grouped by common period (1980-2016) to include all datasets, long-term (1959-2016) to examine agreement to the GPCC for much of the temporal domain, and short-term (1980-2020) using the

GPCP v2.3 and CMAP to examine their full temporal domains with respect to the reanalysis datasets (Tables A5-A7).

4.4.1A. Equatorial Africa

The respective reanalysis agreement over the temporal domain was quite spread with each reanalysis' behavior comparable to their respective VP200 anomalies. The ERA5 was found to have the highest correlation values (r = 0.57-0.66) to the independent precipitation datasets over Equatorial Africa with PR anomaly behaviors bounded closer to zero and less anomalous than the JRA-55 and NCEP reanalysis datasets (Figure 8A). While these r-values do not indicate strong agreement with the independent data, they were notably higher than the other reanalysis datasets with the JRA-55 being the worst performer in this region (r = 0.11-0.20) (Table A5).

Further, it was observed that ERA5 and MERRA-2 were wetter than the independent precipitation datasets from the late 1960s to the late 1990s before becoming drier than these datasets in the latter period (Figures 9A and 9B). This could indicate the existence of a quantifiable drying trend in the ERA5 and/or MERRA-2 data that could improve its agreement with the independent data. The NCEP R1 and JRA-55 exhibited more variability than ERA5 during the study period. This made it difficult to assess any trends that could improve their performances since there was no quantifiable linear trend.

The independent precipitation data were found to be in reasonable agreement with each other with r-values between 0.79 and 0.92 for this period. Further, the independent data did not support the variability shown in the NCEP R1 and JRA-55 and were much closer in behavior and magnitude to the ERA5. R-values were found to be much lower for the ERA5 and JRA-55 when evaluating their agreement with the GPCC for 1959-2016 (Table A6). This emphasized the greater uncertainties observed in the reanalysis data prior to the satellite era (e.g., 1958-1979) and the limitations driven by data sparsity in the region.

4.4.1B. Amazon Basin

The ERA5 was the best performer of any of the reanalysis datasets in the Amazon Basin. Further strengthening this conclusion was that the independent precipitation data remained in strong agreement (r = 0.94-0.98) for this period. Comparing the GPCP v2.3 and CMAP data with the ERA5 yielded the highest r-values of the reanalysis datasets (r = 0.88-0.91) with the JRA-55 scoring just under this (r = 0.83-0.86) for the common 1980-2016 period (Table A5). When examining the earlier period, JRA-55 and ERA5 are closer in correlation with the GPCC (r = 0.74) (Table A6). ERA5 appears closer in values from 1959-1974 before becoming anomalously wetter during the 1975-1984 period (Figure 8B).

Another noteworthy finding in this region was the NCEP R1 and NCEP R2's poor performance with r-values between 0.16 and 0.31 for all independent precipitation datasets. The NCEP R1 PR anomaly values are significantly drier for much of the early period until 1976 when it becomes wetter than the other data through the late 1990s. The seemingly erroneous data continues into the 2000s where values become notably drier once more before settling closer to the other data around 2015. The NCEP R2 resembled the same behaviors as NCEP R1, but with more extremely anomalous PR values (Figures 9C and 9D). This behavior is not physically supported in any other dataset including the newest generation of NCEP reanalysis in the CFSR/v2 and aids in explaining the significant difference in behavior of the VP200 compared to the newer reanalysis datasets (Barichivich et al., 2018). By extension, the NCEP R1 and NCEP R2's inability to resolve the modeled precipitation of this region is likely a key contributor to the large disagreement they have with the non-NCEP reanalysis datasets detected in the velocity potential fields in Section 4.3B.

4.4.1C. Equatorial Central Pacific

Reanalysis agreement across the Equatorial Central Pacific improved in the satellite era, as all three full period datasets had sufficient correlations ($r > 0.60$) with the independent precipitation datasets. The primary caveat was the lack of early period performance analysis due to the GPCC's spatial limitations to only land areas. The ERA5 had the highest r-values once again with r-values ranging between 0.83 and 0.89. The JRA-55 reanalysis was not much lower ($r = 0.81$-0.84) while NCEP R1 and R2 performed the worst but had comparatively higher r-values than it did in other regions ($r = 0.56$-0.67) (Table A5). Despite this, the early period featured notable disagreement between the reanalysis datasets with no independent data to lend confidence in the performance analysis (Table A6). The NCEP R1 on average had anomalously high PRs for the first two decades of the period in comparison to the newer reanalysis data (Figures 8C, 9E, and 9F).

Recalling the significantly anomalously negative VP200 that were estimated during this period, it was leveraged that these higher rain rates were dubious and likely were associated with the aforementioned early period bias in the dataset. Further, the NCEP R1 and R2 observed much lower rain rates than the other data since 2015 decreasing confidence in its usefulness even in more current analysis.

4.4.1D. Equatorial Indonesia

The highest confidence in performance and capturing of variability for the entire temporal domain was in the Equatorial Indonesia region where ERA5 was the best performer (r = 0.84-0.91) and the independent precipitation data were in good agreement (r = 0.84-0.94). JRA-55 was the second-best performer in this region (r = 0.76-0.83) with the NCEP R1 and R2 once again were the worst performers (r = 0.47-0.54) (Table A5). Most notably, ERA5 had the highest correlation with the GPCC over any region (r = 0.80) for the 1959-2016 period making it the best performer of the reanalysis datasets over all regions (Table A6). The early period biases continued to plague the NCEP R1 with notably drier PR anomalies on average until the satellite era with little in the way of coherence to variability depicted in the other data (Figures 8D, 9G, and 9H).

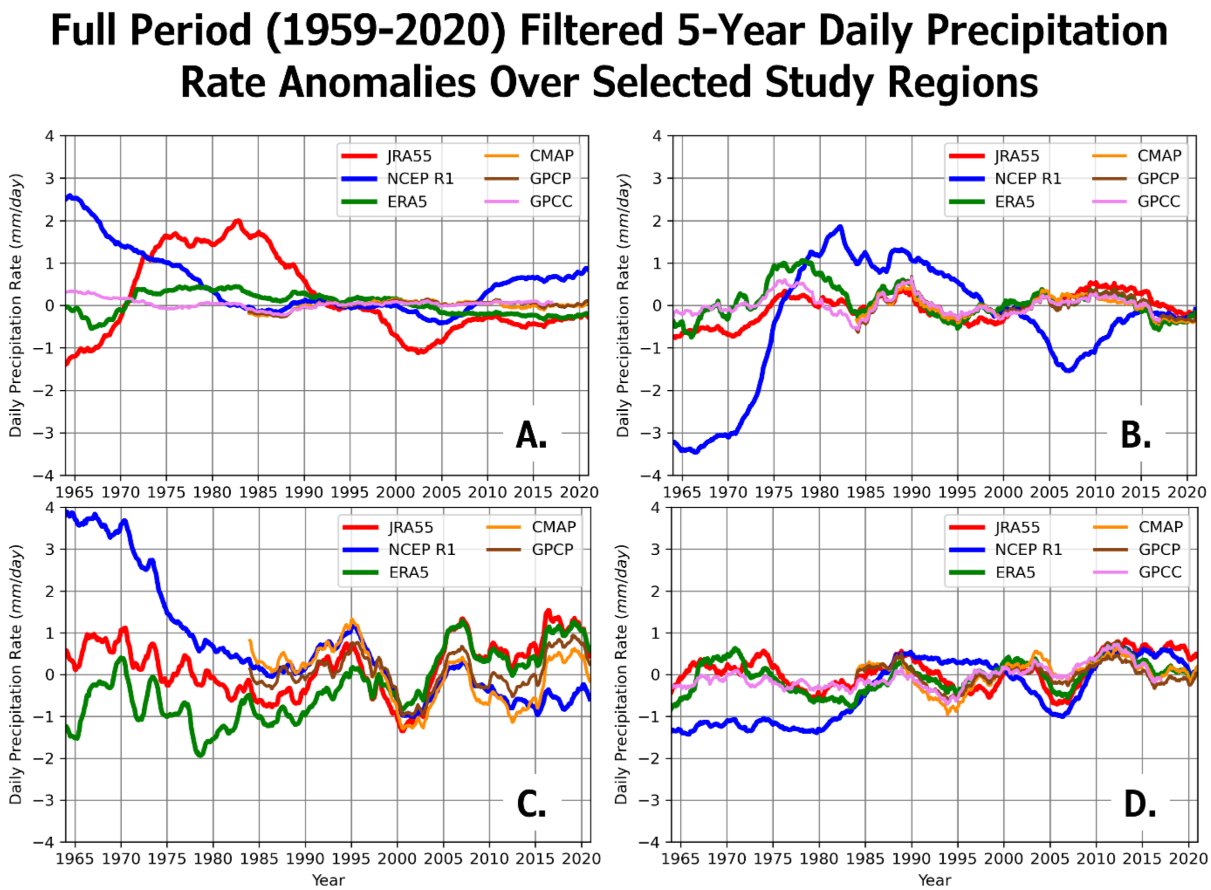

Figure 8. 5-year filtered (moving average) of daily precipitation rate anomalies of each full period global weather reanalysis and independent dataset over (A.) Equatorial Africa, (B.) Amazon Basin, (C.) Equatorial Central Pacific, and (D.) Equatorial Indonesia.

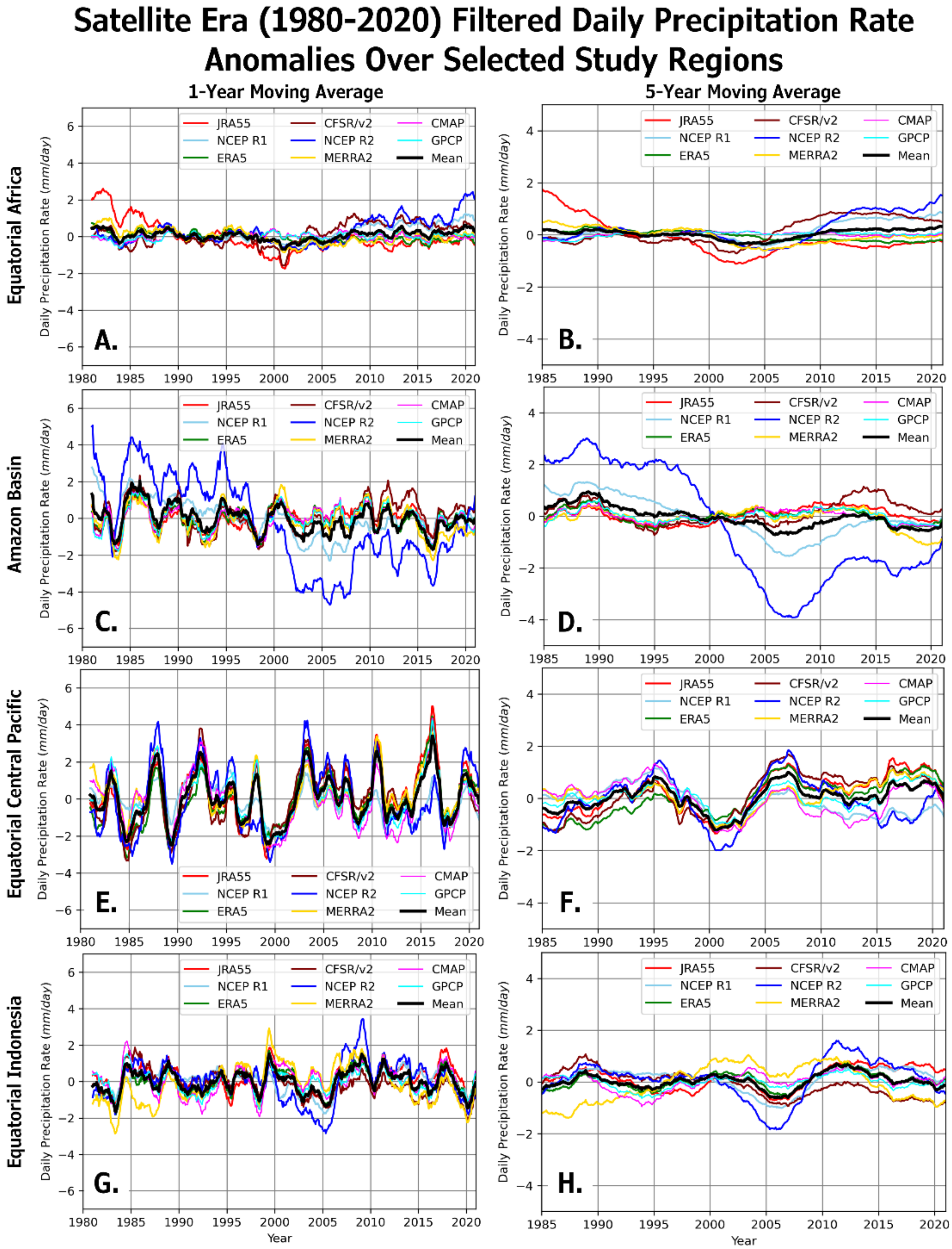

Figure 9. 1-year (left) and 5-year (right) filtered (moving average) of daily precipitation rate anomalies of each global weather reanalysis and independent dataset for only satellite era over (A. and B.) Equatorial Africa, (C. and D.) Amazon Basin, (E. and F.) Equatorial Central Pacific, and (G. and H.) Equatorial Indonesia.

4.4.2. Outgoing Longwave Radiation

The NOAA Interpolated and HIRS OLR datasets did not agree in most regions of this performance analysis. The Equatorial Central Pacific region was the only region where modest agreement existed between the OLR datasets (r = 0.72) with r-values of all other regions at 0.40 or lower (Table A7). Additionally, the NOAA Interpolated OLR dataset had strong disagreement with the full-period reanalysis datasets over all regions while the HIRS OLR dataset exhibited stronger agreement especially with the ERA5. Outside Equatorial Africa, NOAA Interpolated had higher correlations (r = 0.71-0.85) to the satellite era reanalysis datasets through the 1980-2020 period. MERRA-2 and CFSR/v2 in particular being in more agreement with NOAA Interpolated over HIRS OLR indicate the differences in assimilation techniques and data sources that make these data more or less similar to the respective independent OLR datasets. The ERA5 was the best performer over all regions and most notably held a much stronger correlation to the HIRS OLR in the Equatorial Africa region (r = 0.82) compared to the other reanalysis. Most of the conclusions in reanalysis performance were comparable to the precipitation performance analysis which further strengthened the confidence in these conclusions.

4.4.2A. Equatorial Africa

Equatorial Africa had the weakest agreement between OLR datasets (r = 0.08) and the full-period reanalysis data strongly disagreed with the NOAA Interpolated OLR data (r = 0.01-0.08). ERA5 had the strongest agreement with the HIRS OLR data (r = 0.81) with the other reanalysis datasets also having comparatively higher agreement (NCEP R1 r = 0.58, JRA-55 r = 0.50) than with the NOAA Interpolated data (Table A7). The lower correlations with JRA-55 were anticipated given its poor precipitation performance in the precipitation data analysis.

However, conclusions were clouded due to the satellite era reanalysis having higher correlations to the NOAA Interpolated (MERRA-2 r = 0.60, CFSR/v2 r = 0.56, NCEP R2 r = 0.44) rather than HIRS OLR. Given ERA5's correlation to HIRS OLR in addition to the precipitation dataset analysis strengthened confidence in the ERA5 as the best-performing reanalysis dataset in this region (Figures 10A, 11A, and 11B). The primary caveat with this conclusion being that MERRA-2 held the highest correlation to NOAA Interpolated which emphasized the importance of ensemble-based approaches to better capture these uncertainties.

4.4.2B. Amazon Basin

There was poor agreement amongst the full-period reanalysis datasets with the NOAA Interpolated dataset (r = 0.21-0.29) during the 1980-2020 period in the Amazon Basin region while the HIRS OLR data held much stronger agreement. The ERA5 outperformed the other reanalysis datasets (r = 0.91) with JRA-55 as the second-best performer (r = 0.80) (Table A7). NCEP R1's poor precipitation performance in this region extended to OLR with an r-value of 0.51 further decreasing confidence in its reliability for use in estimating variability of VP200 whilst increasing ERA5's confidence in performance over this region (Figures 10B, 11C, and 11D). NOAA Interpolated held highest correlation to CFSR/v2 (r =0.77) and MERRA-2 (r = 0.71) in contrast to the conclusions made by ERA5 using HIRS OLR.

4.4.2C. Equatorial Central Pacific

Independent OLR data was in better agreement with one another in the Equatorial Central Pacific (r = 0.72), however, NOAA Interpolated was still in weaker agreement with the full-period reanalysis datasets (r = 0.51-0.68). Despite the disparities in OLR data, ERA5 was the best performing dataset compared to both independent OLR datasets. The ERA5 had strong agreement with the HIRS OLR data (r = 0.95) followed by the JRA-55 (r = 0.83) and then the NCEP R1 (r = 0.71) (Table A7). NOAA Interpolated's highest agreement was with CFSR/v2 (r = 0.85) and MERRA-2 (r = 0.83), and accounting for agreement with all other datasets in the matrix, these two along with ERA5 were the top performing datasets for this region. These results did not deviate much from the precipitation performances in this region, thus showing a degree of physical and dynamical consistency (Figures 10C, 11E, and 11F).

4.4.2D. Equatorial Indonesia

In conjunction with the precipitation analysis in this region, the ERA5 held the strongest agreement to the independent data (HIRS OLR r = 0.95) compared to the other reanalysis datasets. The HIRS OLR data agreed most with the full-period reanalysis datasets with the NOAA Interpolated in better agreement to the satellite era datasets (r = 0.77-0.79). The JRA-55 was the second-best performer (HIRS OLR r = 0.91) while CFSR/v2 (HIRS OLR r = 0.27) and NCEP R1 (NOAA Int. r = 0.31) were the worst performers in this region (Table A7). Further, the reanalysis datasets were in strongest agreement in this region which was consistent with the correlations computed for precipitation and VP200 (Figures 10D, 11G, and 11H). This yielded the highest confidence of any of the regions that the reanalysis data sufficiently captured variability of the VP200 through much of the study period.

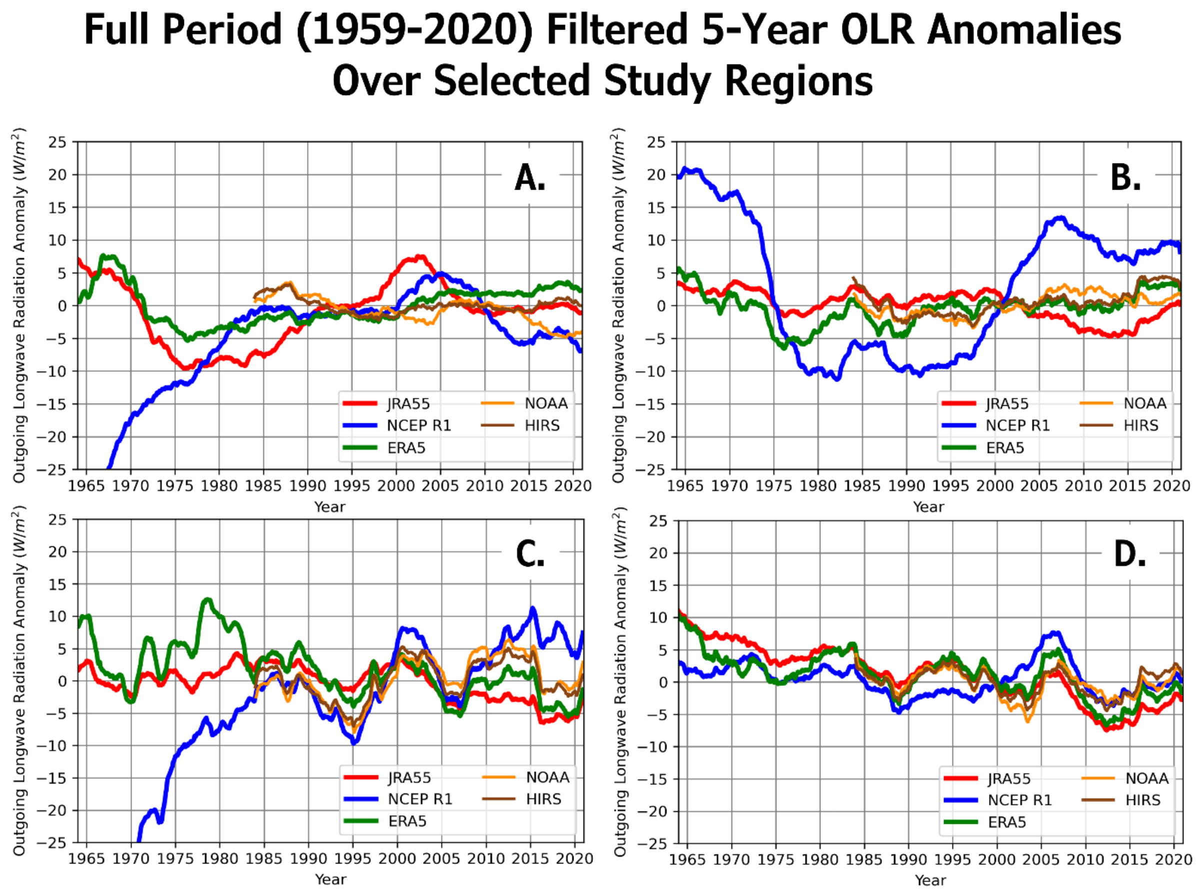

Figure 10. 5-year filtered (moving average) of outgoing longwave radiation anomalies of each full period global weather reanalysis and independent dataset over (A.) Equatorial Africa, (B.) Amazon Basin, (C.) Equatorial Central Pacific, and (D.) Equatorial Indonesia.

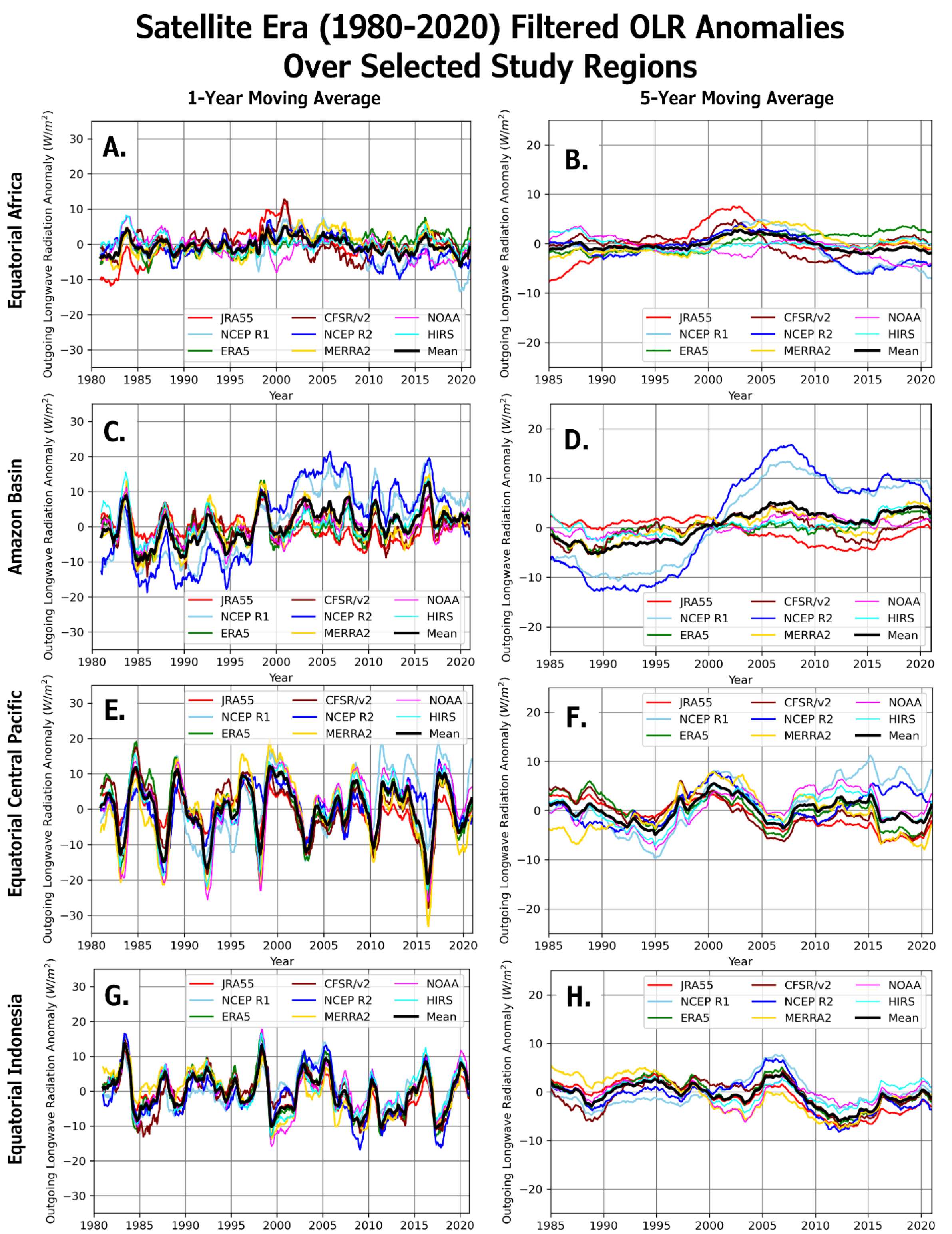

Figure 11. 1-year (left) and 5-year (right) filtered (moving average) of outgoing longwave radiation anomalies of each global weather reanalysis and independent dataset for only satellite era over (A. and B.) Equatorial Africa, (C. and D.) Amazon Basin, (E. and F.) Equatorial Central Pacific, and (G. and H.) Equatorial Indonesia.

5. Conclusion

The development of global weather reanalysis datasets in recent decades has provided the basis for significant advancement in understanding of climate teleconnections and its impacts on tropical convection. The use of VP200 has been popularized for its climate teleconnection applications in both short and long temporal scales with regards to tracking enhancement and suppression of tropical convection and its associated precipitation. Therefore, accurately understanding the variability of VP200 on varying temporal scales in the tropical atmosphere can provide better understanding of how tropical convection is being influenced by tropical overturning circulations (TOCs) on these timescales. Applications such as this could enable more real-time tracking and anticipation of changes in tropical convective behavior as these TOCs change via anthropogenic and natural processes.

The results of this study highlighted the western and eastern equatorial Pacific as the areas of highest agreement while the central equatorial Pacific, equatorial South America, and equatorial Africa as the areas of lowest agreement which strengthened the basis of further analysis of these regions.

After evaluation of key regions of tropical variability, discrepancies in the VP200 magnitude were found to exist between older NCEP/NCAR weather reanalysis datasets and the newer reanalysis such as JRA-55 and ERA5. The largest disagreement was observed in data sparse regions with NCEP R1 observing anomalous VP200 variability in Equatorial Africa, Amazon Basin, and Equatorial Central Pacific, especially prior to 1980. The region with highest agreement across all data sources was Equatorial Indonesia where the largest rising branch of the Global Walker Circulation is situated, and more consistent nearby upper air observations were available. While the discrepancies decreased as the number of observations increased with time, the NCEP R1 and R2 datasets in particular were consistently less correlated with the other reanalysis datasets as well as the independent PR and OLR datasets. The ERA5 reanalysis was consistently the highest correlated to the independent data used in this study, especially over the Amazon Basin, followed by the JRA-55 and MERRA-2. This finding is consistent with other validation studies (Tarek et al. 2020; Hersbach et al. 2020). While these datasets have their own biases that caution exclusive use for future analysis of VP200 variability, they appear to be most representative of VP200 variability over the key regions analyzed. These limitations also highlight the importance of ensemble-based approaches to analyzing variability of climate teleconnections in future studies and its utility in revisiting prior work that used older reanalysis solely. However, selection of reanalysis data sources (i.e. the origin and generation of reanalysis) in any ensemble created is crucial to limit inherent biases.

By establishing the temporal and spatial discrepancies between the data sources in this study, these findings will enable more confident use of global weather reanalysis in further analysis of VP200 variability on varying temporal scales. These discrepancies also highlight the need for continued improvement of weather reanalysis data via increased observations and modeling capabilities as well as more in-depth analysis of specific regions in the tropics (e.g., Eq. Africa) to better understand how these areas influence or are influenced by the TOCs over time.

6. References

Adler, R. F., Sapiano, M. R. P., Huffman, G. J., Wang, J-J., Gu, G., Bolvin, D., Chiu, L., Schneider, U., Becker, A., Nelkin, E., Xie, P., Ferraro, R., Shin, D-B., 2018: The Global Precipitation Climatology Project (GPCP) Monthly Analysis (New Version 2.3) and a Review of 2017 Global Precipitation. *Atmosphere*, **9**(4):138. https://doi.org/10.3390/atmos9040138

Alves de Oliveira, B. F., M. J. Bottino, P. Nobre, and C. A. Nobre, 2021: Deforestation and climate change are projected to increase heat stress risk in the Brazilian Amazon. *Commun Earth Environ*, **2**, 1–8, https://doi.org/10.1038/s43247-021-00275-8.

American Meteorological Society, 2022: Velocity Potential. *Glossary of Meteorology*, http://glossary.ametsoc.org/wiki/velocity_potential.

Arkin, P. A., 1982: The Relationship Between Interannual Variability in the 200 mb Tropical Wind Field and the Southern Oscillation. *Mon. Wea. Rev.,* **110**, 1393–1404, https://doi.org/10.1175/1520-0493(1982)110<1393:TRBIVI>2.0.CO;2.

Back, L. E., and C. S. Bretherton, 2006: Geographic variability in the export of moist static energy and vertical motion profiles in the tropical Pacific. *Geophysical research letters*, **33**(17).

Becker, A., Finger, P., Meyer-Christoffer, A., Rudolf, B., Schamm, K., Schneider, U., and Ziese, M., 2013: A description of the global land-surface precipitation data products of the Global Precipitation Climatology Centre with sample applications including centennial (trend) analysis from 1901–present. *Earth Syst. Sci. Data*, **5**, 71–99, https://doi.org/10.5194/essd-5-71-2013.

Bell, G. D., and M. Chelliah, 2006: Leading Tropical Modes Associated with Interannual and Multidecadal Fluctuations in North Atlantic Hurricane Activity. *J. Climate*, **19**, 590–612, https://doi.org/10.1175/JCLI3659.1.

Chelliah, M., and G. D. Bell, 2004: Tropical Multidecadal and Interannual Climate Variability in the NCEP–NCAR Reanalysis. *J. Climate*, **17**, 1777–1803, https://doi.org/10.1175/1520-0442(2004)017<1777:TMAICV>2.0.CO;2.

Chemke, R., Polvani, L.M., 2019: Opposite tropical circulation trends in climate models and in reanalyses, *Nat. Geosci.* **12**, 528–532. https://doi.org/10.1038/s41561-019-0383-x

Dhame, S., Taschetto, A., Santoso, A., and Meissner, K., 2020: Indian Ocean warming modulates global atmospheric circulation trends. *Climate Dynamics*, **55**. 10.1007/s00382-020-05369-1.

Emanuel, K. A., Neelin, J. D., and C. S. Bretherton, 1994: On large-scale circulations in convecting atmospheres. *Q. J. R. Meteorol. Soc.,* **120**, 519, https://doi.org/10.1002/qj.49712051902

Gastineau, G., Li, L., and Le Treut, H, 2009: The Hadley and Walker Circulation Changes in Global Warming Conditions Described by Idealized Atmospheric Simulations, *Journal of Climate*, **22**(14), 3993-4013.

Geen, R., S. Bordoni, D. S. Battisti, and K. Hui, 2020: Monsoons, ITCZs, and the Concept of the Global Monsoon. *Reviews of Geophysics*, **58**, e2020RG000700, https://doi.org/10.1029/2020RG000700.

Gill, A. E., 1980: Some simple solutions for heat-induced tropical circulation. *Q.J.R. Meteorol. Soc.*, **106**, 447–462, https://doi.org/10.1002/qj.49710644905.

He, J., and Soden, B. J., 2015: Anthropogenic Weakening of the Tropical Circulation: The Relative Roles of Direct CO2 Forcing and Sea Surface Temperature Change. *J. Climate*, **28**(22), 8728-8742.

Held, I. M., and A. Y. Hou, 1980: Nonlinear Axially Symmetric Circulations in a Nearly Inviscid Atmosphere. *J. Atmos. Sci.,* **37**, 515–533, https://doi.org/10.1175/1520-0469(1980)037<0515:NASCIA>2.0.CO;2.

Held, I. M., 2019. 100 Years of Progress in Understanding the General Circulation of the Atmosphere. *Meteorological Monographs*, **59**, 6.1-6.23.

Hendon, H. H., Wheeler, M. C., and Zhang, C., 2007: Seasonal Dependence of the MJO–ENSO Relationship, *J. Climate*, 20(3), 531-543.

Hersbach, H., and Coauthors, 2020: The ERA5 global reanalysis. *Quarterly Journal of the Royal Meteorological Society*, **146**, 1999–2049, https://doi.org/10.1002/qj.3803.

Hersbach, H., and Coauthors, 2019a: Global reanalysis: goodbye ERA-Interim, hello ERA5. *ECMWF newsletter*, doi:10.21957/vf291hehd7. https://www.ecmwf.int/node/19027.

Higgins, R. W., Leetmaa, A., Xue, Y., and Barnston, A., 2000: Dominant Factors Influencing the Seasonal Predictability of U.S. Precipitation and Surface Air Temperature. *J. Climate*, **13**, 3994–4017, https://doi.org/10.1175/1520-0442(2000)013<3994:DFITSP>2.0.CO;2.

Holton, J.R., 2004: *Introduction to Dynamic Meteorology*. 4th Edition, Elsevier, Amsterdam, 535 p.

Jiang, X., A.F. Adames, D. Kim, E.D. Maloney, H. Lin, H. Kim, C. Zhang, C.A. DeMott, and N.P. Klingaman, 2020: Fifty years of research on the Madden-Julian Oscillation: Recent progress, challenges, and perspectives. *Journal of Geophysical Research: Atmospheres,* **125**(17), e2019JD030911.

Kalnay, E., and Coauthors, 1996: The NCEP/NCAR 40-Year Reanalysis Project, *Bulletin of the American Meteorological Society*, 77(3), 437-472.

Kinter, J. L., Fennessy, M. J., Krishnamurthy, V., and Marx, L., 2004: An Evaluation of the Apparent Interdecadal Shift in the Tropical Divergent Circulation in the NCEP–NCAR Reanalysis. *J. Climate*, **17**, 349–361, https://doi.org/10.1175/1520-0442(2004)017<0349:AEOTAI>2.0.CO;2.

Kistler, R., and Coauthors., 2001: The NCEP–NCAR 50-Year Reanalysis: Monthly Means CD-ROM and Documentation. *Bulletin of the American Meteorological Society*, **82**(2), 247-268.

Kobayashi, S., and Coauthors, 2015: The JRA-55 Reanalysis: General Specifications and Basic Characteristics. *Journal of the Meteorological Society of Japan,* **93**. 5-48. 10.2151/jmsj.2015-001.

Krishnamurti, T. N., 1971: Observational study of the tropical upper tropospheric motion field during the Northern Hemisphere summer. *J. Appl. Meteor.,***10**, 1066–1096.

Lau, W. K., Waliser, D. E., & Waliser, D., 2005: *Predictability and forecasting* (pp. 389-423). Springer Berlin Heidelberg.

Lee, H.-T., A. Gruber, R. G. Ellingson and I. Laszlo, 2007: Development of the HIRS Outgoing Longwave Radiation climate data set, *J. Atmos. Ocean. Tech.,* **24**, 2029–2047.

Lee, H.-T., 2018: Quality Assurance Summary and Results for Monthly and Daily OLR CDR (rev.20180831).

Liebmann, B., and C. A. Smith, 1996: Description of a complete (interpolated) outgoing longwave radiation dataset. *Bull. Amer. Meteor. Soc.,* **77**, 1275–1277

Ma, J., Xie, S., and Kosaka, Y., 2012: Mechanisms for Tropical Tropospheric Circulation Change in Response to Global Warming. *J. Climate*, **25**(8), 2979-2994.

Ma, K., Chadwick, R., Seo, K., Dong, C., Huang, G., Foltz, G.R., Jiang, J. H., 2018: Responses of the Tropical Atmospheric Circulation to Climate Change and Connection to the Hydrological Cycle. *Annual Review of Earth and Planetary Sciences,* **46:1**, 549-580.

Madden, R. A., and P. R. Julian, 1971: Detection of a 40-50 day oscillation in the zonal wind in the tropical Pacific. *J. Atmos. Sci*., **28**, 702-708.

Madden, R. A., and P. R. Julian, 1972: Description of Global-Scale Circulation Cells in the Tropics with a 40–50 Day Period. *J. Atmos. Sci.,* **29**, 1109–1123, https://doi.org/10.1175/1520-0469(1972)029<1109:DOGSCC>2.0.CO;2.

McPhaden, M. J., Zhang, X., Hendon, H. H., and Wheeler, M. C., 2006: Large scale dynamics and MJO forcing of ENSO variability, *Geophys. Res. Lett.,* **33**, L16702, doi:10.1029/2006GL026786.

Newman, M., Sardeshmukh, P. D., and Bergman, J. W., 2000: An Assessment of the NCEP, NASA, and ECMWF Reanalyses over the Tropical West Pacific Warm Pool, *Bulletin of the American Meteorological Society,* **81**(1), 41-48.

Oliver, J. E., 2005: Walker Circulation. Encyclopedia of World Climatology. Ed. by JE Oliver. Dordrecht: Springer Netherlands, 797-798.

Raj, J., H. K. Bangalath, and G. Stenchikov, 2019: West African Monsoon: current state and future projections in a high-resolution AGCM. *Clim Dyn*, **52**, 6441–6461, https://doi.org/10.1007/s00382-018-4522-7.

Roundy, P. E., 2015: On the Interpretation of EOF Analysis of ENSO, Atmospheric Kelvin Waves, and the MJO. *J. Climate*, **28**, 1148-1165.

Roundy, P. E., MacRitchie, K., Asuma, J., and Melino, T., 2010: Modulation of the Global Atmospheric Circulation by Combined Activity in the Madden–Julian Oscillation and the El Niño–Southern Oscillation during Boreal Winter. *J. Climate*, **23**, 4045–4059, https://doi.org/10.1175/2010JCLI3446.1.

Roundy, P. E., and Schreck III, C.J., 2009: A combined wave-number-frequency and time-extended EOF approach for tracking the progress of modes of large-scale organized tropical convection. *Q. J. R. Meteorol. Soc.,* **135**, 161-173.

Roundy, P. E., Schreck III, C.J., Janiga, M.A., 2009: Contributions of convectively coupled equatorial Rossby waves and Kelvin waves to the Real-time multivariate MJO indices. *Mon. Wea. Rev*., **137**, 469-478.

Schreck, C. J., H.-T. Lee and K. Knapp, 2018: HIRS Outgoing Longwave Radiation—Daily Climate Data Record: Application toward Identifying Tropical Subseasonal Variability. *Remote Sens*, **10**, 1325; https://doi.org/10.3390/rs10091325

Seidel, D. J., Q. Fu, W. J. Randel, and T. J. Reichler, 2008: Widening of the tropical belt in a changing climate, *Nat. Geosci*., **1**, 21– 24.

Tanaka, H. L., Ishizaki, N., and Kitoh, A., 2004: Trend and interannual variability of Walker, monsoon and Hadley circulations defined by velocity potential in the upper troposphere. *Tellus A: Dynamic Meteorology and Oceanography*, **56:3**, 250-269, DOI: 10.3402/tellusa.v56i3.14410

Tarek, M., F. P. Brissette, and R. Arsenault, 2020: Evaluation of the ERA5 reanalysis as a potential reference dataset for hydrological modelling over North America. *Hydrology and Earth System Sciences*, **24**, 2527–2544, https://doi.org/10.5194/hess-24-2527-2020.

Trenberth, K. E., Stepaniak, D. P., and Caron, J. M., 2000: The Global Monsoon as Seen through the Divergent Atmospheric Circulation, *J. Climate*, 13(22), 3969-3993.

Vecchi, G. A., & Soden, B. J., 2007: Global Warming and the Weakening of the Tropical Circulation. *J. Climate*, 20(17), 4316-4340.

Ventrice, M. J., M. C. Wheeler, H. H. Hendon, C. J. Schreck, C. D. Thorncroft, and G. N. Kiladis, 2013: A Modified Multivariate Madden–Julian Oscillation Index Using Velocity Potential. *Mon. Wea. Rev.,* 141, 4197–4210, https://doi.org/10.1175/MWR-D-12-00327.1.

Ventrice, M.J., C. D. Thorncroft, and P. E. Roundy, 2011: The Madden-Julian Oscillation's influence on African easterly waves and downstream tropical cyclogenesis. *Mon. Wea. Rev.,* 139, 2704–2722.

Walker, G.T. and E. W. Bliss, 1930: World Weather IV, *Memoirs of the Royal Meteorological Society*, 3, (24), 81–95.

Wheeler, M., and Hendon, H., 2004: An All-Season Real-Time Multivariate MJO Index: Development of an Index for Monitoring and Prediction. *Mon. Wea. Rev.,* 132. 1917-1932. 10.1175/1520-0493(2004)132<1917:AARMMI>2.0.CO;2.

Xie, P., and P.A. Arkin, 1997: Global precipitation: A 17-year monthly analysis based on gauge observations, satellite estimates, and numerical model outputs. Bull. Amer. Meteor. Soc., 78, 2539 – 2558

Zaitchik, B. F., 2017: Madden-Julian Oscillation impacts on tropical African precipitation. *Atmospheric Research*, 184, 88-102.

Zhang, Y., J. M. Wallace, and D. S. Battisti, 1997: ENSO-like Interdecadal Variability: 1900–93. *J. Climate*, 10, 1004–1020, https://doi.org/10.1175/1520-0442(1997)010<1004:ELIV>2.0.CO;2.

Zhang, Y., and Wang, K., 2021: Global precipitation system size. *Environmental Research Letters*, 16(5), 054005.

Appendix A – Tables

Reanalysis 200 hPa Velocity Potential Variable R-values by 10^{o} Intervals – 1959-2020 Moving 30^{o} Longitudinal Averages				
Longitude	**JRA55:NCEP R1**	**JRA55:ERA5**	**ERA5:NCEP R1**	**Mean Value**
0-30^{o}E	0.46	0.70	0.41	0.52
10-40^{o}E	0.48	0.71	0.44	0.54
20-50^{o}E	0.58	0.73	0.49	0.60
30-60^{o}E	0.68	0.75	0.57	0.67
40-70^{o}E	0.75	0.76	0.63	0.71
50-80^{o}E	0.79	0.74	0.65	0.73
60-90^{o}E	***0.81***	0.72	0.62	0.72
70-100^{o}E	***0.82***	0.73	0.62	0.72
80-110^{o}E	***0.84***	0.77	0.66	0.76
90-120^{o}E	***0.87***	***0.81***	0.72	***0.80***
100-130^{o}E	***0.89***	***0.84***	0.78	***0.84***
110-140^{o}E	***0.89***	***0.86***	0.79	***0.85***
120-150^{o}E	***0.88***	***0.84***	0.77	***0.83***
130-160^{o}E	***0.83***	0.78	0.68	0.76
140-170^{o}E	0.76	0.71	0.53	0.67
150-180^{o}E	0.69	0.69	0.41	0.60
160-190^{o}E	0.67	0.73	0.38	0.59
170-200^{o}E	0.68	0.78	0.42	0.63
180-210^{o}E	0.70	***0.81***	0.46	0.66
190-220^{o}E	0.73	***0.82***	0.50	0.68
200-230^{o}E	0.76	***0.83***	0.56	0.72
210-240^{o}E	***0.81***	***0.85***	0.67	0.78
220-250^{o}E	***0.87***	***0.87***	0.76	***0.83***
230-260^{o}E	***0.90***	***0.87***	***0.80***	***0.86***
240-270^{o}E	***0.88***	***0.83***	0.75	***0.82***
250-280^{o}E	***0.85***	0.76	0.67	0.76
260-290^{o}E	***0.80***	0.62	0.56	0.66
270-300^{o}E	0.76	0.46	0.46	0.56
280-310^{o}E	0.75	0.35	0.38	0.49
290-320^{o}E	0.74	0.35	0.33	0.47
300-330^{o}E	0.71	0.40	0.29	0.47
310-340^{o}E	0.65	0.46	0.28	0.46
320-350^{o}E	0.61	0.53	0.28	0.47
330-0^{o}E	0.60	0.61	0.31	0.51
340-10^{o}E	0.59	0.65	0.33	0.52
350-20^{o}E	0.57	0.69	0.37	0.54

Table A1. R-values describing the level of reanalysis agreement of VP200 over 30^{o} moving longitudinal averages.

Reanalysis 200 hPa Velocity Potential Annual Climatological Means (*10^5 m^2/s)			
Equatorial Africa			
Climate Period	**JRA55**	**ERA5**	**NCEP R1**
1971-2000	3.58	4.64	7.96
1981-2010	4.42	4.99	7.47
1991-2020	4.96	5.17	6.61
Amazon Basin			
Climate Period	**JRA55**	**ERA5**	**NCEP R1**
1971-2000	3.00	1.79	0.12
1981-2010	2.61	1.97	0.50
1991-2020	2.67	2.35	1.74
Equatorial Central Pacific			
Climate Period	**JRA55**	**ERA5**	**NCEP R1**
1971-2000	-3.46	-2.95	-5.78
1981-2010	-3.30	-3.15	-5.09
1991-2020	-3.33	-3.30	-5.14
Equatorial Indonesia			
Climate Period	**JRA55**	**ERA5**	**NCEP R1**
1971-2000	-9.29	-9.51	-10.20
1981-2010	-9.62	-9.64	-10.27
1991-2020	-10.02	-9.95	-10.14

Table A2. Annual climatological means of VP200 for each global weather reanalysis for the last three 30-year climate periods.

Reanalysis 200 hPa Velocity Potential Variable R-values Matrix – 1959-2020				
Equatorial Africa				
	JRA55	**ERA5**	**NCEP R1**	**Mean**
JRA55	1.00	0.83	0.54	0.69
ERA5	0.83	1.00	0.64	***0.74***
NCEP R1	0.54	0.64	1.00	0.54
Mean	0.69	***0.74***	0.54	-
Equatorial Amazon				
	JRA55	**ERA5**	**NCEP R1**	**Mean**
JRA55	1.00	0.92	0.61	0.77
ERA5	0.92	1.00	0.71	***0.82***
NCEP R1	0.61	0.71	1.00	0.66
Mean	0.66	***0.82***	0.66	-
Equatorial Central Pacific				
	JRA55	**ERA5**	**NCEP R1**	**Mean**
JRA55	1.00	0.97	0.88	***0.93***
ERA5	0.97	1.00	0.85	0.91
NCEP R1	0.88	0.85	1.00	0.87
Mean	***0.93***	0.91	0.87	-
Equatorial Indonesia				
	JRA55	**ERA5**	**NCEP R1**	**Mean**
JRA55	1.00	0.98	0.86	***0.92***
ERA5	0.98	1.00	0.84	0.91
NCEP R1	0.86	0.84	1.00	0.85
Mean	***0.92***	0.91	0.85	-

Table A3. R-value matrix describing the level of full period reanalysis agreement of VP200 over the four study regions analyzed.

Reanalysis 200 hPa Velocity Potential Variable R-values Matrix – 1980-2020							
Equatorial Africa							
	JRA55	**ERA5**	**NCEP R1**	**CFSR/v2**	**NCEP R2**	**MERRA-2**	**Mean**
JRA55	1.00	0.90	0.58	0.61	0.61	0.78	0.70
ERA5	0.90	1.00	0.69	0.69	0.72	0.84	***0.77***
NCEP R1	0.58	0.69	1.00	0.45	0.97	0.61	0.66
CFSR/v2	0.61	0.69	0.45	1.00	0.47	0.62	0.57
NCEP R2	0.61	0.72	0.97	0.47	1.00	0.65	0.68
MERRA-2	0.78	0.84	0.61	0.62	0.65	1.00	0.70
Mean	0.70	***0.77***	0.66	0.57	0.68	0.70	-
Amazon Basin							
	JRA55	**ERA5**	**NCEP R1**	**CFSR/v2**	**NCEP R2**	**MERRA-2**	**Mean**
JRA55	1.00	0.92	0.61	0.68	0.72	0.85	0.76
ERA5	0.92	1.00	0.71	0.70	0.76	0.90	***0.80***
NCEP R1	0.61	0.71	1.00	0.51	0.90	0.77	0.70
CFSR/v2	0.68	0.70	0.51	1.00	0.56	0.65	0.62
NCEP R2	0.72	0.76	0.90	0.56	1.00	0.79	0.75
MERRA-2	0.85	0.90	0.77	0.65	0.79	1.00	0.79
Mean	0.76	***0.80***	0.70	0.62	0.75	0.79	-
Equatorial Central Pacific							
	JRA55	**ERA5**	**NCEP R1**	**CFSR/v2**	**NCEP R2**	**MERRA-2**	**Mean**
JRA55	1.00	0.97	0.88	0.78	0.88	0.90	***0.88***
ERA5	0.97	1.00	0.85	0.81	0.85	0.87	0.87
NCEP R1	0.88	0.85	1.00	0.67	0.95	0.84	0.84
CFSR/v2	0.78	0.81	0.67	1.00	0.63	0.75	0.73
NCEP R2	0.88	0.85	0.95	0.63	1.00	0.81	0.82
MERRA-2	0.90	0.87	0.84	0.75	0.81	1.00	0.83
Mean	***0.88***	0.87	0.84	0.73	0.82	0.83	-
Equatorial Indonesia							
	JRA55	**ERA5**	**NCEP R1**	**CFSR/v2**	**NCEP R2**	**MERRA-2**	**Mean**
JRA55	1.00	0.98	0.86	0.87	0.86	0.90	***0.89***
ERA5	0.98	1.00	0.84	0.87	0.84	0.89	0.88
NCEP R1	0.86	0.84	1.00	0.80	0.98	0.84	0.86
CFSR/v2	0.87	0.87	0.80	1.00	0.78	0.77	0.82
NCEP R2	0.86	0.84	0.98	0.78	1.00	0.85	0.86
MERRA-2	0.90	0.89	0.84	0.77	0.85	1.00	0.85
Mean	***0.89***	0.88	0.86	0.82	0.86	0.85	-

Table A4. R-value matrix describing the level of satellite era reanalysis agreement over the four study regions analyzed.

Reanalysis Precipitation Variable R-values Matrix – 1980-2020									
Equatorial Africa									
	JRA55	**ERA5**	**NCEP R1**	**CFSR/v2**	**NCEP R2**	**MERRA-2**	**CMAP**	**GPCP**	**Mean**
JRA55	1.00	0.57	0.25	0.32	0.19	0.57	0.11	0.18	0.31
ERA5	0.57	1.00	0.25	0.33	0.26	0.73	***0.56***	***0.65***	0.48
NCEP R1	0.25	0.25	1.00	0.61	0.81	0.31	0.22	0.32	0.40
CFSR/v2	0.32	0.33	0.61	1.00	0.53	0.44	0.38	0.47	0.44
NCEP R2	0.19	0.26	0.81	0.53	1.00	0.40	0.25	0.33	0.40
MERRA-2	0.57	0.73	0.31	0.44	0.40	1.00	0.45	0.50	0.49
CMAP	0.11	***0.56***	0.22	0.38	0.25	0.45	1.00	0.83	0.40
GPCP	0.18	***0.65***	0.32	0.47	0.33	0.50	0.83	1.00	0.47
Mean	0.31	0.48	0.40	0.44	0.40	0.49	0.40	0.47	-
Amazon Basin									
	JRA55	**ERA5**	**NCEP R1**	**CFSR/v2**	**NCEP R2**	**MERRA-2**	**CMAP**	**GPCP**	**Mean**
JRA55	1.00	0.85	0.26	0.75	0.22	0.78	0.84	0.85	0.65
ERA5	0.85	1.00	0.29	0.80	0.33	0.85	0.87	0.90	***0.70***
NCEP R1	0.26	0.29	1.00	0.18	0.57	0.31	0.17	0.21	0.28
CFSR/v2	0.75	0.80	0.18	1.00	0.33	0.77	0.81	0.84	0.64
NCEP R2	0.22	0.33	0.57	0.33	1.00	0.36	0.28	0.31	0.34
MERRA-2	0.78	0.85	0.31	0.77	0.36	1.00	0.80	0.84	0.67
CMAP	0.84	0.87	0.17	0.81	0.28	0.80	1.00	0.96	0.68
GPCP	0.85	0.90	0.21	0.84	0.31	0.84	0.96	1.00	0.70
Mean	0.65	***0.70***	0.28	0.64	0.34	0.67	0.68	0.70	-
Equatorial Central Pacific									
	JRA55	**ERA5**	**NCEP R1**	**CFSR/v2**	**NCEP R2**	**MERRA-2**	**CMAP**	**GPCP**	**Mean**
JRA55	1.00	0.90	0.65	0.86	0.64	0.85	0.82	0.84	***0.79***
ERA5	0.90	1.00	0.53	0.90	0.61	0.85	0.83	0.89	***0.79***
NCEP R1	0.65	0.53	1.00	0.57	0.68	0.59	0.67	0.62	0.62
CFSR/v2	0.86	0.90	0.57	1.00	0.61	0.81	0.80	0.84	0.77
NCEP R2	0.64	0.61	0.68	0.61	1.00	0.55	0.56	0.59	0.61
MERRA-2	0.85	0.85	0.59	0.81	0.55	1.00	0.85	0.85	0.76
CMAP	0.82	0.83	0.67	0.80	0.56	0.85	1.00	0.93	0.78
GPCP	0.84	0.89	0.62	0.84	0.59	0.85	0.93	1.00	0.79
Mean	***0.79***	***0.79***	0.62	0.77	0.61	0.76	0.78	0.79	-
Equatorial Indonesia									
	JRA55	**ERA5**	**NCEP R1**	**CFSR/v2**	**NCEP R2**	**MERRA-2**	**CMAP**	**GPCP**	**Mean**
JRA55	1.00	0.90	0.69	0.75	0.67	0.74	0.81	0.83	0.77
ERA5	0.90	1.00	0.66	0.80	0.65	0.86	0.88	0.92	***0.81***
NCEP R1	0.69	0.66	1.00	0.64	0.81	0.53	0.50	0.54	0.62
CFSR/v2	0.75	0.80	0.64	1.00	0.59	0.68	0.74	0.80	0.71
NCEP R2	0.67	0.65	0.81	0.59	1.00	0.54	0.47	0.53	0.61
MERRA-2	0.74	0.86	0.53	0.54	0.54	1.00	0.79	0.80	0.69
CMAP	0.81	0.88	0.50	0.74	0.47	0.79	1.00	0.94	0.73
GPCP	0.83	0.92	0.54	0.80	0.53	0.80	0.94	1.00	0.77
Mean	0.77	***0.81***	0.62	0.71	0.61	0.69	0.73	0.77	-

Table A5. R-value matrix describing the level of reanalysis agreement to each independent precipitation dataset over the four study regions for the common period (1980-2020).

Reanalysis Precipitation Variable R-values Matrix – 1959-2016 (Full Period Only)				
Equatorial Africa				
	JRA55	**ERA5**	**NCEP R1**	**GPCC**
JRA55	1.00	0.54	-0.10	0.06
ERA5	0.54	1.00	0.08	0.39
NCEP R1	-0.10	0.08	1.00	0.40
GPCC	0.06	0.39	0.40	1.00
Amazon Basin				
	JRA55	**ERA5**	**NCEP R1**	**GPCC**
JRA55	1.00	0.66	0.29	***0.74***
ERA5	0.66	1.00	0.26	***0.74***
NCEP R1	0.29	0.26	1.00	0.16
GPCC	***0.74***	***0.74***	0.16	1.00
Equatorial Central Pacific				
	JRA55	**ERA5**	**NCEP R1**	**GPCC**
JRA55	1.00	0.78	0.47	N/A
ERA5	0.78	1.00	0.27	N/A
NCEP R1	0.47	0.27	1.00	N/A
GPCC	N/A	N/A	N/A	N/A
Equatorial Indonesia				
	JRA55	**ERA5**	**NCEP R1**	**GPCC**
JRA55	1.00	0.77	0.54	0.66
ERA5	0.77	1.00	0.54	***0.80***
NCEP R1	0.54	0.54	1.00	0.42
GPCC	0.66	***0.80***	0.42	1.00

Table A6. R-value matrix describing the level of full period reanalysis agreement to the GPCC precipitation dataset over the four study regions (1959-2016).

Reanalysis Outgoing Longwave Radiation Variable R-values Matrix – 1980-2020									
Equatorial Africa									
	JRA55	**ERA5**	**NCEP R1**	**CFSR/ v2**	**NCEP R2**	**MERRA-2**	**NOAA**	**HIRS**	**Mean**
JRA55	1.00	0.61	0.57	0.22	0.19	0.27	0.01	0.50	0.34
ERA5	0.61	1.00	0.52	0.02	0.02	0.21	0.04	***0.82***	0.32
NCEP R1	0.57	0.52	1.00	0.10	0.35	0.23	0.08	0.58	0.35
CFSR/v2	0.22	0.02	0.10	1.00	0.52	0.62	0.56	0.00	0.29
NCEP R2	0.19	0.02	0.35	0.52	1.00	0.52	0.43	0.03	0.29
MERRA-2	0.27	0.21	0.23	0.62	0.52	1.00	***0.61***	0.10	0.37
NOAA	0.01	0.04	0.08	0.56	0.43	***0.61***	1.00	0.08	0.26
HIRS	0.50	***0.82***	0.58	0.00	0.03	0.10	0.08	1.00	0.30
Mean	0.34	0.32	0.35	0.29	0.29	0.37	0.26	0.30	-
Amazon Basin									
	JRA55	**ERA5**	**NCEP R1**	**CFSR/ v2**	**NCEP R2**	**MERRA-2**	**NOAA**	**HIRS**	**Mean**
JRA55	1.00	0.80	0.31	0.19	-0.05	0.25	0.21	0.80	0.36
ERA5	0.80	1.00	0.48	0.21	0.19	0.29	0.29	***0.91***	0.45
NCEP R1	0.31	0.48	1.00	0.18	0.57	0.35	0.28	0.51	0.38
CFSR/v2	0.19	0.21	0.18	1.00	0.53	0.55	***0.77***	0.23	0.38
NCEP R2	-0.05	0.19	0.57	0.53	1.00	0.49	0.54	0.24	0.36
MERRA-2	0.25	0.29	0.35	0.55	0.49	1.00	0.71	0.32	0.42
NOAA	0.21	0.29	0.28	***0.77***	0.54	0.71	1.00	0.33	0.45
HIRS	0.80	***0.91***	0.51	0.24	0.24	0.32	0.33	1.00	0.48
Mean	0.36	0.45	0.38	0.38	0.36	0.42	0.45	0.48	-
Equatorial Central Pacific									
	JRA55	**ERA5**	**NCEP R1**	**CFSR/ v2**	**NCEP R2**	**MERRA-2**	**NOAA**	**HIRS**	**Mean**
JRA55	1.00	0.89	0.57	0.57	0.28	0.55	0.51	0.83	0.60
ERA5	0.89	1.00	0.62	0.65	0.34	0.63	0.69	***0.95***	***0.68***
NCEP R1	0.57	0.62	1.00	0.36	0.40	0.49	0.53	0.70	0.52
CFSR/v2	0.57	0.65	0.36	1.00	0.47	0.81	***0.85***	0.61	0.62
NCEP R2	0.28	0.34	0.40	0.47	1.00	0.50	0.55	0.40	0.42
MERRA-2	0.55	0.63	0.49	0.81	0.50	1.00	0.83	0.66	0.64
NOAA	0.51	0.69	0.53	***0.85***	0.55	0.83	1.00	0.72	0.67
HIRS	0.83	***0.95***	0.70	0.61	0.40	0.66	0.72	1.00	0.70
Mean	0.60	***0.68***	0.52	0.62	0.42	0.64	0.67	0.70	-
Equatorial Indonesia									
	JRA55	**ERA5**	**NCEP R1**	**CFSR/ v2**	**NCEP R2**	**MERRA-2**	**NOAA**	**HIRS**	**Mean**
JRA55	1.00	0.95	0.75	0.31	0.39	0.47	0.41	0.91	***0.60***
ERA5	0.95	1.00	0.80	0.31	0.39	0.42	0.41	***0.95***	***0.60***
NCEP R1	0.75	0.80	1.00	0.29	0.40	0.33	0.31	0.77	0.52
CFSR/v2	0.31	0.31	0.29	1.00	0.78	0.68	0.77	0.27	0.49
NCEP R2	0.39	0.39	0.40	0.78	1.00	0.85	0.78	0.33	0.55
MERRA-2	0.47	0.42	0.33	0.68	0.76	1.00	***0.79***	0.40	0.55
NOAA	0.41	0.41	0.31	0.77	0.78	***0.79***	1.00	0.41	0.55
HIRS	0.91	***0.95***	0.77	0.27	0.33	0.40	0.41	1.00	0.58
Mean	***0.60***	***0.60***	0.52	0.49	0.55	0.55	0.55	0.58	1.00

Table A7. R-value matrix describing the level of reanalysis agreement to each independent outgoing longwave radiation dataset over the four study regions for the common period (1980-2020).